



UNIVERSITY OF LEEDS

This is a repository copy of *Re-Os age constraints and new observations of Proterozoic glacial deposits in the Vazante Group, Brazil*.

White Rose Research Online URL for this paper:  
<http://eprints.whiterose.ac.uk/80332/>

Version: Submitted Version

---

**Article:**

Geboy, NJ, Kaufman, AJ, Walker, RJ et al. (6 more authors) (2013) Re-Os age constraints and new observations of Proterozoic glacial deposits in the Vazante Group, Brazil. *Precambrian Research*, 238. 199 - 213. ISSN 0301-9268

<https://doi.org/10.1016/j.precamres.2013.10.010>

---

**Reuse**

Unless indicated otherwise, fulltext items are protected by copyright with all rights reserved. The copyright exception in section 29 of the Copyright, Designs and Patents Act 1988 allows the making of a single copy solely for the purpose of non-commercial research or private study within the limits of fair dealing. The publisher or other rights-holder may allow further reproduction and re-use of this version - refer to the White Rose Research Online record for this item. Where records identify the publisher as the copyright holder, users can verify any specific terms of use on the publisher's website.

**Takedown**

If you consider content in White Rose Research Online to be in breach of UK law, please notify us by emailing [eprints@whiterose.ac.uk](mailto:eprints@whiterose.ac.uk) including the URL of the record and the reason for the withdrawal request.



[eprints@whiterose.ac.uk](mailto:eprints@whiterose.ac.uk)  
<https://eprints.whiterose.ac.uk/>

1 **Re-Os age constraints and new observations of Proterozoic glacial deposits in the Vazante Group,**  
2 **Brazil**

3  
4 Nicholas J. Geboy<sup>1</sup>, Alan J. Kaufman<sup>2,3</sup>, Richard J. Walker<sup>2</sup>, Aroldo Misi<sup>4</sup>, Tolentino Flavio de Oliveira<sup>5</sup>,  
5 Kristen E. Miller<sup>6</sup>, Karem Azmy<sup>7</sup>, Brian Kendall<sup>8</sup>, and Simon W. Poulton<sup>9</sup>  
6

7 1. United States Geological Survey, Reston, VA 20192, USA

8 2. University of Maryland, Department of Geology, College Park, MD 20742, USA

9 3. University of Maryland, Earth System Science Interdisciplinary Center, College Park, MD 20742, USA

10 4. Centro de Pesquisa em Geofisica e Geologia, Universidade Federal da Bahia (CPGG/UFBA), CEP 40170-290  
11 Salvador-Bahia, Brazil

12 5. Independent consultant, Rio de Janeiro RJ, Brazil

13 6. Massachusetts Institute of Technology, Department of Earth, Atmospheric and Planetary Sciences, Cambridge,  
14 MA 02139, USA

15 7. Department of Earth Sciences, Memorial University of Newfoundland, St. John's, Newfoundland A1B 3X5,  
16 Canada

17 8. University of Waterloo, Department of Earth and Environmental Sciences, Waterloo, Ontario N2L 3G1,  
18 CANADA

19 9. University of Leeds, School of Earth and Environment, Leeds LS2 9JT, United Kingdom  
20

21 **ABSTRACT**

22 A new Re-Os radiometric age date for an organic-rich shale horizon from the Vazante Group in Brazil,  
23 coupled with geological observations, provide evidence for late Mesoproterozoic glacial episodes,  
24 conflicting with the general view of greenhouse conditions marked by a eustatic high stand at this time.  
25 Field observations of a reverse fault juxtaposing older Mesoproterozoic sedimentary rocks above younger  
26 Neoproterozoic strata provide a new stratigraphic framework and reconcile the apparent inversion of U-  
27 Pb detrital zircon ages through the succession. Combined, the geochronological, geochemical and

28 stratigraphic evidence suggest that the Vazante Group sediments accumulated along a passive margin of  
29 the São Francisco craton and are correlative with the neighboring Paranoá Group. Biomarker, sulfur  
30 isotope and iron speciation analyses support the interpretation of a strongly stratified water column during  
31 post-glacial transgression and deposition of one of the bituminous shale horizons. The relationship of the  
32 glaciogenic Vazante Group to other late Mesoproterozoic successions, such as the non-glacial Atar Group  
33 in West Africa and Bylot Supergroup in arctic Canada, however, remains enigmatic.

34

35 Key words: Vazante Group; Mesoproterozoic glaciation; Re-Os geochronology; Fe-speciation

36

### 37 **1. Introduction**

38 The Precambrian geologic record contains evidence of widespread ice ages, including diamictite  
39 left behind by melting glaciers, capped by texturally and isotopically anomalous carbonate and organic-  
40 rich shale that accumulated in the wake of rising sea levels (Harland and Bidgood, 1959; Kaufman et al.,  
41 1991; Kirschvink, 1992; Kennedy 1996; Hoffman et al., 1998; Schrag et al., 2002; Bekker et al., 2005).  
42 Existing age constraints suggest that these Precambrian ice ages were episodic rather than continuous,  
43 with a series of temporally discrete glaciation events occurring at the beginning and end of the  
44 Proterozoic Eon (*cf.* Kaufman et al., 1997; Kennedy et al., 1998; Walter et al., 2000; Kendall et al., 2004;  
45 2006) but with little evidence of glaciation in the intervening billion years.

46 Due to the general lack of radiometric determinations on sedimentary successions, however, the  
47 absolute ages of many of the Proterozoic diamictites are poorly known. To advance understanding of the  
48 tempo and mode of these ancient ice ages, researchers have applied a geochronometer based on the  
49 radioactive decay of  $^{187}\text{Re}$  to  $^{187}\text{Os}$ , most commonly on samples of organic-rich shale preserved in drill  
50 cores (Kendall et al., 2004; 2006; Azmy et al., 2008; Rooney et al., 2010) or syn-depositional sulfide  
51 grains (Hannah et al., 2004). Published results for Neoproterozoic (1.0-0.542 Ga) successions support the  
52 view that the Sturtian and Marinoan glacial epochs represented multiple discrete ice ages over a  
53 protracted time frame (*cf.* Kaufman et al., 1997). Contrary to expectations, a Re-Os study of a dropstone-

54 laden shale horizon from the Vazante Group in south-central Brazil (Azmy et al., 2008) indicated a late  
55 Mesoproterozoic age – a time previously believed to have been ice free.

56 In this paper, we re-evaluate the stratigraphic position of this shale, which was previously  
57 interpreted to be syn-glacial in origin (Olcott et al., 2005) and support the Mesoproterozoic age with new  
58 Re-Os work from a second shale horizon unrelated to glacial deposits, as well as identify a thrust fault  
59 lower in the Vazante Group that juxtaposes older Mesoproterozoic strata above younger glaciogenic  
60 sedimentary rocks of Neoproterozoic age. Detrital zircon U-Pb constraints for the Vazante Group  
61 (Rodrigues et al., 2012), coupled with carbon and strontium isotope data and paleontological evidence,  
62 are consistent with the stratigraphic inversion and our Re-Os age determinations.

63

## 64 **2. Geologic and Geochronologic Background**

65 The Vazante Group is a sedimentary succession that occurs in wide swaths atop the eastern part  
66 of the Brasília Fold Belt (BFB) on the western margin of the São Francisco craton throughout Minas  
67 Gerais, Brazil (Fig. 1). Surface outcrops are strongly weathered and the succession has been exposed to  
68 sub-greenschist facies metamorphism (Babinski et al., 2005; Azmy et al., 2008), but well preserved  
69 carbonate and organic-rich shale are available in drill core. Figure 2 shows a generalized stratigraphy of  
70 the Vazante Group, including three potential glacial horizons, as well as the reverse fault located near the  
71 town of Lagamar (Pinho and Dardenne, 1994), which resulted in older strata of the Vazante Group –  
72 including the shale horizons studied here – to overly younger sedimentary rocks (see Section 5.1 for  
73 further details and implications). The basal Vazante diamictite (St. Antônio do Bonito Formation) has  
74 long been interpreted as glacial in origin based on the presence of faceted and striated cobbles of mixed  
75 lithology, including basement clasts, floating in a mudstone matrix (Dardenne, 2000). The two upper  
76 Vazante Group diamictites at the base of the Morro do Calcário and Lapa formations are characterized by  
77 carbonate breccia or laminated shale disrupted by carbonate dropstones. Further evidence for a glacial  
78 origin for the two upper Vazante diamictites includes: 1) their widespread distribution across the basin; 2)  
79 the observation that cobbles and boulders in the Morro do Calcário (previously attributed to the Serra do

80 Poço Verde Formation) are both rounded and angular, with the rounded stones often faceted (Fig. 3A, B);  
81 3) the thick black Morro do Calcário shale contains glendonite, a pseudomorph of ikaite, a carbonate  
82 mineral that forms in organic-rich sediment at temperatures between -1.9 to 7°C (*cf.* Olcott et al., 2005);  
83 4) the uppermost strata of the Lapa diamictite are Fe-oxide cemented with local accumulations of iron-  
84 formation (*cf.* Derry et al., 1992; Kaufman et al., 1997; Hoffman et al., 1998); and 5) the carbonates and  
85 marl overlying both diamictites preserve negative  $\delta^{13}\text{C}$  excursions typical of post-glacial cap carbonates  
86 (Azmy et al., 2001; 2006; Brody et al., 2004).

87         The three shale horizons sampled for Re-Os analysis in this study were from, in ascending order,  
88 the pre-glacial Serra do Garrote Formation and the post-glacial Morro do Calcário and Lapa formations.  
89 The Serra do Garrote Formation consists of dark grey shale hundreds of meters thick that has been  
90 metamorphosed to a greenish slate in some areas; the shale can be carbonaceous and/or pyrite bearing  
91 (Dardenne, 2000). The Morro do Calcário and Lapa formations are both composed of laminated shale  
92 and dolostone, which contain intermittent ice-rafted debris and based on core observations are each  
93 several hundred meters thick (Dardenne, 2000). The true thickness of these units, however, is difficult to  
94 ascertain insofar as outcrops are discontinuous and coupled with the likelihood of tectonic repetition of  
95 strata due to thrust faulting. The Morro do Calcário and Lapa formations accumulated during post-glacial  
96 transgression over sub-glacial valleys largely filled with carbonate breccia. Sub-glacial unconformities cut  
97 through underlying carbonate platform deposits of the Serra do Poço Verde and Morro do Calcário  
98 formations (indicated by the heavier formation-boundary lines in Fig. 2); in some cores it appears that the  
99 two upper Vazante Group diamictites are in direct contact while in others they are separated by a variety  
100 of bedded lithologies.

101         The age of the Vazante Group is controversial. Cloud and Dardenne (1973) argued that the  
102 presence of the stromatolite *Conophyton metula Kirichenko* (Fig. 3C) near the base of the Lagamar  
103 Formation suggests an age ranging between 1350 and 950 Ma. Stromatolite biostratigraphy, however, is  
104 poorly constrained and competing tectonic models suggest a Neoproterozoic initiation of Vazante Group  
105 sedimentation either in a rapidly subsiding foreland basin associated with the Brasília collision (*ca.* 790

106 Ma; Dardenne, 2000) or along a passive continental margin during supercontinent breakup (*ca.* 900 Ma;  
107 Pimentel et al., 2001). Whole rock Rb-Sr data for a Vazante Group shale yielded an isochron age of ~600  
108 Ma, but this age likely represents a date related to Brasíliao metamorphism (Amaral and Kawashita,  
109 1967). A Neoproterozoic age for the upper Vazante Group was suggested based on a comparison of time-  
110 series isotope trends (Azmy et al., 2001), although an alternative interpretation of these variations  
111 suggested an older potential age for the succession (Misi et al., 2007). Most recently, Re-Os dates of 993  
112  $\pm 46$  and  $1100 \pm 77$  Ma (excluding Re- and Os-poor samples) were determined from a dropstone-laden  
113 shale in the Vazante Group previously believed to be part of the Lapa Formation (Azmy et al., 2008) but  
114 here is assigned to the Morro do Calcário Formation (see below).

115

### 116 **3. Methods**

117 All samples were taken from two pristine drill cores provided by Votorantim Metais. For Re-Os  
118 analysis, samples were selected from the Serra do Garrote Formation in drill hole 134-86, from roughly  
119 coeval horizons of the Morro do Calcário Formation in drill holes 42-88 and 134-86 and from the Lapa  
120 Formation in drill hole 134-86. The upper two shale horizons in core 134-86 are separated by a thick  
121 interval of carbonate breccia, quartzite and iron-cemented diamictite (Brody et al., 2004). In 2009, we re-  
122 examined this core and concluded that the shale horizon Azmy et al. (2008) studied from drill hole  
123 MASW-01 belonged to the Morro do Calcário Formation, rather than the Lapa Formation as previously  
124 discussed.

125

#### 126 *3.1 Re/Os*

127 The Re-Os system can provide precise depositional ages for organic-rich shale because these  
128 facies are often deposited in anoxic environments where Re and, to a lesser extent, Os may be sequestered  
129 from seawater in their reduced states and incorporated into organic matter (Ravizza and Turekian, 1989;  
130 Cohen et al., 1999; Selby and Creaser, 2003; Kendall et al., 2004). Once incorporated in the sediment,  
131  $^{187}\text{Re}$  undergoes beta decay to  $^{187}\text{Os}$  with a half-life of approximately ~42 Ga. With the assumption that

132 all of the shale samples in a suite have the same initial osmium isotopic composition (from coeval  
133 seawater) and a wide range in parent:daughter ratios, it is possible to generate an isochron, which yields  
134 the age of incorporation of Re and Os into the system and, hence, of deposition. Since shale facies  
135 contain both hydrogenous and terrigenous components, it is necessary to digest the samples with a less-  
136 aggressive medium, such as  $\text{Cr}^{\text{VI}}\text{-H}_2\text{SO}_4$ , which preferentially attacks the organic component while  
137 leaving the detrital quartz and feldspar largely intact (Selby and Creaser, 2003).

138         Approximately 50 mg of powdered whole rock was accurately weighed along with a known  
139 quantity of a  $^{190}\text{Os}\text{-}^{185}\text{Re}$  spike and  $\text{Cr}^{\text{VI}}\text{-H}_2\text{SO}_4$  digestion solution (Selby and Creaser, 2003) and  
140 transferred to frozen Carius tubes that were chilled using a mixture of dry ice and ethanol before being  
141 sealed with an oxy-propane torch (Shirey and Walker, 1995). Once thawed, the Carius tubes were placed  
142 in an oven heated to  $240^\circ\text{C}$  for 48 hours to fully oxidize the Re and Os to their highest valence states.  
143 Following digestion, the tubes were frozen in liquid nitrogen and opened. The Os was separated from the  
144 mixture via solvent extraction using carbon tetrachloride, back extracted into HBr and purified by micro-  
145 distillation prior to being loaded onto a Pt filament and analyzed using negative thermal ionization mass  
146 spectrometry (N-TIMS; Birck et al., 1997; Cohen and Waters, 1996). Following Os separation, the  
147 remaining solution was treated with sulfurous acid to reduce the  $\text{Cr}^{6+}$  to  $\text{Cr}^{3+}$ , and Re was separated using  
148 anion exchange chromatography before being taken up in 2% nitric acid and analyzed using inductively  
149 coupled plasma mass spectrometry (ICP-MS). All of the preparation chemistry and spectrometry were  
150 conducted at the University of Maryland's Geochemical Laboratories. Samples were blank corrected,  
151 with total analytical blanks averaging 19 pg and  $< 1$  pg for Re and Os, respectively. These blanks were  
152 sufficiently low as to have no effect on analytical uncertainties. Reproducibility was determined using a  
153  $^{185}\text{Re}$  spiked in-house standard of the Agpalilik iron meteorite, where  $^{185}\text{Re}/^{187}\text{Re} = 1.331 \pm 0.002$  ( $n = 10$ ;  
154 2SDM) over a two-month measuring period and a UMD Os standard where  $^{187}\text{Os}/^{188}\text{Os} = 0.1140 \pm 0.0003$   
155 ( $n = 9$ ; 2SDM) and  $^{190}\text{Os}/^{192}\text{Os} = 1.981 \pm 0.002$  ( $n = 9$ ; 2SDM) over a nine-month measuring period.  
156 Regressions were performed with *Isoplot V.4.15* (Ludwig, 2011) using a value of  $1.666 \times 10^{-11} \text{ yr}^{-1}$  for the

157  $^{187}\text{Re}$  decay constant and  $2\sigma$  uncertainties for  $^{187}\text{Re}/^{188}\text{Os}$  and  $^{187}\text{Os}/^{188}\text{Os}$  as determined by numerical  
158 error propagation.

159

### 160 *3.2 Total Organic Carbon and Stable Isotopes*

161 Shale horizons were sampled from drill cores 134-86 and 42-88 for time-series analyses.  
162 Samples were ground with a ceramic mortar and pestle and aliquots were used for measuring total organic  
163 carbon (TOC) abundance, stable S and C isotope analyses, as well as Fe-speciation. TOC was determined  
164 using Dumas combustion techniques on pre-acidified powders and quantified on a vacuum distillation  
165 line. The  $\delta^{13}\text{C}$  of the TOC was determined by combustion in a Eurovector elemental analyzer in-line with  
166 an Isoprime gas source isotope ratio mass spectrometer (EA-IRMS). Sulfide sulfur in the shales was  
167 isolated using a chrome-reduction solution (*cf.* Canfield et al., 1986) to release  $\text{H}_2\text{S}$ , which was carried in  
168 a stream of nitrogen gas through a Milli-Q ultrapure water trap to remove chloride. Sulfur was then  
169 trapped as  $\text{Ag}_2\text{S}$  with a 0.02 M solution of  $\text{AgNO}_3$  and 1.55 M  $\text{HNO}_3$ . Silver sulfide solutions were set in  
170 the dark for approximately seven days, then filtered and rinsed with ~250 ml Milli-Q water and ~5 ml 1N  
171 ammonia solution ( $\text{NH}_4\text{OH}$ ). Samples were aged to allow for the dissolution of oxygen-bearing  
172 contaminants that precipitate with the silver sulfide. The black  $\text{Ag}_2\text{S}$  precipitate was then filtered and  
173 dried for ~48 hours and combined with excess  $\text{V}_2\text{O}_5$  in tin cups for EA-IRMS measurement of sulfur  
174 isotope compositions. Uncertainties of carbon and sulfur isotope analyses based on multiple analyses of  
175 urea and NBS-127 standards were better than 0.1 and 0.3‰, respectively.

176

### 177 *3.3 Fe-Speciation*

178 Iron-speciation analyses, based on measured abundances of Fe in carbonate, oxide and sulfide  
179 mineral phases, as well as total Fe in samples, were conducted following procedures outlined by Poulton  
180 and Canfield (2005). Sulfide iron abundance (Fe-S) is calculated from  $\text{Ag}_2\text{S}$  yields in CRS extractions  
181 (see Section 3.2), performed sequentially after checking for Fe present as acid volatile sulfides. For the  
182 carbonate and oxide fractions, fresh bulk powders are sequentially leached with: 1) 1 M sodium acetate

183 (C<sub>2</sub>H<sub>3</sub>NaO<sub>2</sub>) adjusted to pH 4.5 with acetic acid (CH<sub>3</sub>COOH) for 48 hours at 50°C to release carbonate  
184 iron (Fecarb); 2) dithionite solution (mixture of 50 g L<sup>-1</sup> sodium dithionite (Na<sub>2</sub>S<sub>2</sub>O<sub>4</sub>), 0.2 M sodium  
185 citrate (Na<sub>3</sub>C<sub>6</sub>H<sub>5</sub>O<sub>7</sub>•H<sub>2</sub>O) and 0.35 M acetic acid) for two hours to release iron from ferric oxides such as  
186 hematite and goethite (Fe<sub>ox</sub>); and 3) ammonium oxalate solution (mixture of 0.2 M ammonium oxalate  
187 (C<sub>2</sub>H<sub>8</sub>N<sub>2</sub>O<sub>4</sub>) and 0.17 M oxalic acid (H<sub>2</sub>C<sub>2</sub>O<sub>4</sub>•H<sub>2</sub>O) for six hours to extract iron from magnetite (Fe<sub>mag</sub>).  
188 The iron extracted from carbonates, oxides and sulfides are combined to yield the highly reactive pool  
189 (Fe<sub>HR</sub>). This Fe<sub>HR</sub> pool represents Fe minerals that are reactive towards dissolved sulfide on diagenetic  
190 timescales (Canfield et al., 1992; Poulton et al., 2004a). Total iron concentrations (Fe<sub>T</sub>) were determined  
191 by total digestion with concentrated HF, HNO<sub>3</sub> and HClO<sub>4</sub>. All Fe extracts were analysed by Flame  
192 Atomic Adsorption Spectroscopy, with repeat analyses yielding RSD's of <5% for all stages.

193

## 194 **4. Results**

195

### 196 *4.1 Re-Os*

197 Results of Re and Os analyses for the Serra do Garrote, Morro do Calcário and Lapa formation  
198 shales are reported in Table 1. In the Serra do Garrote samples, Re and Os concentrations ranged from ~1  
199 to 16 ppb, and ~60 to 600 ppt, respectively. The isotopic data show a generally isochronous relationship  
200 (Fig. 4A) indicating an age of 1354 ± 88 Ma (n = 8, MSWD = 49). Presuming the isochron age to be  
201 accurate, the initial <sup>187</sup>Os/<sup>188</sup>Os value (Os<sub>i</sub>) of each sample is back-calculated. The reproducibility of Os<sub>i</sub>  
202 of individual samples in the Serra do Garrote shale (Table 1) suggests minimal post-depositional mobility  
203 (Kendall et al., 2009). The Serra do Garrote date presented here is, admittedly, imprecise with a relatively  
204 high MSWD value. However, the Os<sub>i</sub> from the isochron regression falls between values of ~0.12  
205 (chondritic/mantle compositions in the late Mesoproterozoic; Walker et al., 2002a, b) and 1.5 (riverine  
206 inputs; Levasseur et al., 1999) that would reasonably be expected for seawater <sup>187</sup>Os/<sup>188</sup>Os. Such an  
207 observation suggests that any post-depositional disturbance is relatively minor. The large uncertainty  
208 (~5%) on the age may arise from changes in the initial Os isotopic composition of seawater during

209 deposition (data used to generate Fig. 4A come from samples spreading approximately 1.5 m of section).

210 The changing Os isotopic composition of the source water and minor open-system behavior may also

211 explain the relatively high MSWD value.

212 Rhenium and Os concentrations in the thick, organic-rich Morro do Calcário shale vary  
213 substantially between the two sampled cores, which were drilled ~2.3 km apart. Samples from drill core  
214 42-88 contain between ~0.30 and 0.85 ppb Re and between ~27 and 55 ppt Os, while those from drill core  
215 134-86 are characterized by higher concentrations with ~1 to 23 ppb Re and ~40 to 700 ppt Os. The  
216 differences are most likely related to environmental and facies variations, as metal abundances in the two  
217 cores are broadly correlated with that of total organic carbon, suggesting sedimentary controls on their  
218 distribution (Anbar et al., 2007). Sample sets from these two cores can be combined to yield a composite  
219 isochron with an age of  $1112 \pm 50$  Ma ( $n = 16$ , MSWD = 91; Fig. 4B). Although care was taken to  
220 sample the two drill cores from roughly equivalent horizons, we cannot *a priori* assume that these  
221 horizons are directly contemporaneous, particularly as the data plot in two distinct positions along the  
222 isochron. Furthermore, the samples from drill core 42-88 have very low Re and Os abundances, and  
223 therefore may be more readily contaminated by detrital components of the shale (Azmy et al., 2008).  
224 Taking only the more metal enriched Morro do Calcário samples from drill core 134-86 results in an  
225 imprecise isochron age of  $1035 \pm 200$  Ma ( $n = 8$ , MSWD = 150; Fig. 4C) with scatter that is greater than  
226 analytical uncertainties. Duplicate analyses of some samples gave minor to moderate differences in  
227  $^{187}\text{Re}/^{188}\text{Os}$  and  $^{187}\text{Os}/^{188}\text{Os}$  and likely reflect variable extents of powder heterogeneity. While neither the  
228 composite isochron nor the drill core 134-86 isochron are strong enough to warrant a direct depositional  
229 age assignment, it is worth noting that both are statistically identical to the Morro do Calcário  
230 Formation's previously assigned Re-Os age ( $1100 \pm 77$  Ma; Azmy et al., 2008).

231 Samples from the thin Lapa Formation shale in core 134-86 have the lowest concentrations of  
232 both Re and Os in this study (Table 1), and exhibit a very limited range in  $^{187}\text{Re}/^{188}\text{Os}$  and  $^{187}\text{Os}/^{188}\text{Os}$ .  
233 Hence, these samples do not define an isochron, and we do not consider the Lapa Formation  
234 measurements further.

235

#### 236 4.2 C-S

237 Results for time-series C and S analyses from the Serra do Garrotte, Morro do Calcário and Lapa  
238 formations sampled from drill core 134-86 and 42-88 are reported in Table 2 and illustrated in Figures 5  
239 and 6. In core 134-86 (Fig. 5), where all three shale horizons were collected and analyzed, TOC  
240 abundances range widely between 0 and 4 wt.% with highest overall (but variable) abundances in the  
241 Morro do Calcário shale and in a singular peak within the Lapa shale. Carbon isotope compositions of  
242 Serra do Garrotte samples range between -28 and -31‰, values similar to samples from the base of the  
243 Morro do Calcário Formation. Stratigraphically higher in the Morro do Calcário, samples define a trend  
244 of  $^{13}\text{C}$  enrichment with  $\delta^{13}\text{C}$  values reaching as high as -22‰. In contrast, organic matter in Lapa  
245 Formation samples have relatively constant  $\delta^{13}\text{C}$  values around -25‰. Sulfur isotope compositions in this  
246 core were not measured for the Serra do Garrotte Formation. In the Morro do Calcário, sample  $\delta^{34}\text{S}$   
247 values range from +10 to -15‰, becoming more depleted in  $^{34}\text{S}$  up-section. In contrast, Lapa Formation  
248 samples are notably enriched in  $^{34}\text{S}$ , ranging from +10 to +35‰, defining a positive excursion that peaks  
249 in the most organic-rich horizons.

250 Morro do Calcário samples from core 42-88 (Fig. 6) were previously studied for biomarker  
251 distributions and organic carbon contents (Olcott et al., 2005). TOC abundances in these samples range  
252 up to 3.5 wt.%, with most samples having  $\delta^{13}\text{C}$  values near to -25‰, regardless of organic carbon content.  
253 Sulfur contents are similar to those of organic matter, ranging up to 3 wt.%, but  $\delta^{34}\text{S}$  values define a  
254 significant positive excursion with a progressive 20‰ rise in the lower half of the section to values as  
255 high as approximately +30‰, which fall back to around +10‰ in the upper half of the section.

256

#### 257 4.3 Fe-speciation

258 Iron-speciation analyses were conducted on the Morro do Calcário samples from core 42-88 (Fig.  
259 6; Table 3) in order to better understand the redox architecture of the depositional basin and for

260 comparison with environmental interpretations from the previously published biomarker results.  $Fe_{HR}/Fe_T$   
261 ratios can be used to distinguish oxic from anoxic water column depositional conditions, whereby values  
262  $>0.38$  provide strong support for anoxic deposition, while values  $<0.22$  suggest oxic depositional water  
263 column conditions (Raiswell and Canfield, 1998; Poulton and Raiswell, 2002; Poulton and Canfield,  
264 2011). For samples that show clear evidence for anoxic deposition,  $Fe-S/Fe_{HR}$  values  $>0.7-0.8$  suggest  
265 euxinic deposition, while values below this threshold suggest anoxic non-sulfidic depositional conditions  
266 (Poulton et al., 2004b; Poulton and Canfield, 2011).  $Fe_{HR}/Fe_T$  ratios range widely through the formation  
267 (Fig. 6). Notably high values for samples at depths  $<759$  m, between 785 and 812 m, and  $>825$  m provide  
268 strong evidence for dominantly anoxic deposition across these intervals, perhaps with occasional  
269 transitions to oxic deposition from 800-812 m (potentially a consequence of fluctuations in the depth of  
270 the chemocline). In contrast, low  $Fe_{HR}/Fe_T$  from 759-785 m and 812-825 m depths suggests dominantly  
271 oxic water column conditions for these samples, although periodically higher  $Fe_{HR}/Fe_T$  ratios suggest the  
272 possibility of cycling between oxic and anoxic conditions. To distinguish anoxic non-sulfidic and euxinic  
273 deposition,  $Fe-S/Fe_{HR}$  ratios are plotted on Fig. 6 for samples which show evidence of anoxic deposition  
274 (i.e.,  $Fe_{HR}/Fe_T > \sim 0.38$ ). In general, lower  $Fe-S/Fe_{HR}$  towards the top and bottom of the section implies  
275 anoxic non-sulfidic depositional conditions, while higher values in the middle portion of the section  
276 suggests dominantly euxinic conditions.

277

## 278 **5. Discussion**

279 Although the Re-Os isochron ages for upper Vazante shales determined previously (Azmy et al.,  
280 2008) and in this study are imprecise, they are consistent with a late Mesoproterozoic to earliest  
281 Neoproterozoic age assignment. This age for the Vazante Group contrasts with an earlier  
282 chemostratigraphic age estimate (Azmy et al., 2001; 2006), which was in part based on the assumption  
283 that all the glacial deposits must be from the Neoproterozoic Era.

284

285 *5.1 Stratigraphic context for a Mesoproterozoic age of the upper Vazante Group*

286 Detrital zircons from the middle of the Serra do Garrote and the top of the Morro do Calcário  
287 formations yield U-Pb ages varying from 1505 to 2521 Ma and 1109 to 2466 Ma, respectively; lower in  
288 the Serra do Garrote detrital zircon ages vary from 1242 to 3409 Ma (Rodrigues et al., 2012). Taken as  
289 maximum depositional ages, these former dates do not contradict the Re-Os ages but do require relatively  
290 rapid unroofing and transportation of the zircons. In contrast, younger detrital zircon U-Pb ages from  
291 formations of the Vazante Group below the shale horizons (Azmy et al., 2008; Rodriguez et al., 2012) do  
292 appear to contradict our Re-Os age estimates. For example, the Rocinha Formation contains zircons as  
293 young as 930 Ma and the St. Antônio do Bonito Formation contains zircons with ages as young as ~1000  
294 Ma (Azmy et al., 2008; Rodrigues et al., 2012), suggesting a likely Neoproterozoic age for this part of the  
295 succession. In support of this view, Sr isotope compositions of phosphorite samples from the Rocinha  
296 Formation (Fig. 3D), with  $^{87}\text{Sr}/^{86}\text{Sr}$  values of 0.70766 (Misi et al., 2007), match those of the  
297 Neoproterozoic Bambuí Group to the east on the São Francisco craton. The cap carbonate at the base of  
298 that succession is constrained by a Pb-Pb carbonate age of  $740 \pm 22$  Ma ( $n = 11$ ; MSWD = 0.66; Babinski  
299 et al., 2007).

300 These paradoxical observations are resolved by the presence of a 40-45° oblique-slip reverse fault  
301 beneath outcrops of *Conophyton metula Kirichenko* stromatolite in the Lagamar Formation (Fig. 3E).  
302 The fault is identified in aerial photographs and in the field by the presence of brown to yellow clay-rich  
303 and sandy mylonite overlying thickly bedded purple shale (Fig. 3F). This reverse fault appears to  
304 subdivide the Vazante Group into two parts; older sediments assigned to the Vazante Group are thrust  
305 above younger carbonates and phosphates in the Rocinha Formation and the St. Antônio do Bonito  
306 Formation glacial diamictite (Misi et al., 2010; 2011). Notably, the Vazante Formation (now Group)  
307 originally defined by Dardenne (1978) did not include the basal Santo Antônio do Bonito and Rocinha  
308 because these units were severely faulted relative to overlying strata. This tectonic transposition explains  
309 many of the conflicting chronometric constraints on the Vazante Group and should be expected given the  
310 imbrication of thrust nappes to the west and south in highly metamorphosed terrains (Dardenne, 2000).  
311 Movement along this reverse fault – initiated by collision of continental blocks during the late-

312 Neoproterozoic (*ca.* 600 Ma) Brasíliao orogeny – places older strata above younger and separates the  
313 Vazante Group into at least two distinct tectonic and sedimentary domains. If this interpretation is  
314 correct, the basal Vazante Group diamictite would likely be equivalent to the glacial deposits at the base  
315 of the Neoproterozoic Bambuí Group, leaving the two glacial deposits above the thrust fault to be the only  
316 radiometrically constrained glaciogenic deposits of the Mesoproterozoic Era. The possibility of  
317 additional, yet unrecognized, reverse faults in the Vazante Group cannot be discounted, which may  
318 explain the slightly younger U-Pb ages observed in detrital zircons in the lower part of the Serra do  
319 Garrote Formation (Rodrigues et al., 2012).

320

### 321 *5.2 Regional and depositional setting of the Vazante Group*

322 Two different tectonic models have been proposed to explain the accumulation of Vazante Group  
323 strata. In one, Vazante sediments are suggested to have been deposited in a rapidly subsiding foreland  
324 basin initiated during collision of the BFB with the flat-lying São Francisco craton at *ca.* 790 Ma  
325 (Dardenne, 2000). This suggests a Neoproterozoic age for the succession. However, accepting the Re-Os  
326 and U-Pb detrital zircon age constraints, as well as the presence of a major reverse fault within the  
327 Vazante succession, it is most likely that only the Rocinha Formation and St. Antônio do Bonito  
328 diamictite are correlative with Neoproterozoic deposits on the São Francisco craton (Misi et al., 2010;  
329 2011).

330 In contrast, upper Vazante Group strata that accumulated on a passive margin carbonate platform  
331 are of Mesoproterozoic age and likely correlative with the Paranoá Group (Fig 1) consistent with the  
332 interpreted model based on Nd isotopic measurements of detrital grains from a variety of formations  
333 across the BFB (Pimentel et al., 2001). The Nd-isotope measurements suggest a likely source of  
334 sediments to the Vazante Group was from either the São Francisco craton to the east ( $T_{DM}$  ranging from  
335  $\sim 2.3$  to  $1.7$  Ga) or the off-shore Goiás Magmatic Arc to the west ( $T_{DM}$  ranging from  $\sim 1.0$  to  $1.3$  Ga). The  
336 initial Nd isotopic compositions of detrital grains from the Serra do Garrote and Serra do Poço Verde  
337 formations are identical to those from the nearby Paranoá Group, supporting their direct equivalence

338 (Pimentel et al., 2001). The Paranoá Group lacks direct radiometric constraints but is broadly constrained  
339 to between 1200 and 900 Ma (albeit based on stromatolite biostratigraphy; Dardenne et al., 1976). The  
340 Paranoá Group sits stratigraphically below the Bambuí Group, and glacial deposits have also been  
341 observed at its base (Dardenne, 2000). Carbonates in both the Vazante and Paranoá groups reveal  
342 relatively little  $\delta^{13}\text{C}$  variation (Santos et al., 2000; Azmy et al., 2001). The pattern of relatively muted  
343 carbon isotope compositions through these successions stands in sharp contrast with Neoproterozoic  
344 carbonates of the Bambuí Group which exhibit a striking upsection trend in  $\delta^{13}\text{C}$  values progressing from  
345 as low as -5‰ near its base in a cap carbonate lithofacies to near +15‰ at its top in bituminous  
346 limestones (Misi et al., 2007).

347         Previous biomarker studies of the Morro do Calcário shale (Olcott et al., 2005) interpreted this  
348 unit to be syn-glacial based on its appearance between thick carbonate diamictite and ample evidence of  
349 ice rafted debris. We currently recognize this organic-rich shale as related to post-glacial transgression  
350 with a stratigraphic placement between two carbonate diamictites of different age. Extractable  
351 biomarkers (including n-alkanes, isoprenoids, steranes and hopanes from shale, carbonate and diamictite)  
352 in the Morro do Calcário shale were interpreted to be indigenous to the sediments and reflect a complex  
353 microbial ecosystem, including both phototrophic bacteria and eukaryotes living in a stratified ocean with  
354 thin or absent sea ice, oxic surface waters and euxinic conditions within the photic zone (Olcott et al.,  
355 2005). Our Fe-speciation and S isotope results from the Morro do Calcário shale are consistent with these  
356 findings. The partitioning of Fe phases in these ancient sediments suggest that redox conditions in the  
357 depositional environment fluctuated on relatively short timescales between anoxic, euxinic and oxic water  
358 column conditions as the Morro do Calcário sediments accumulated, supporting the view of initial  
359 progressive stratification of the water column followed by generally more expansive ventilation. The  
360 dramatic enrichment in  $^{34}\text{S}$  of pyrite in the lower part of the sampled interval may thus be interpreted in  
361 terms of progressive sulfate-limitation as the water column became increasingly euxinic. Our re-  
362 evaluation of this shale as a post-glacial (rather than syn-glacial) deposit, however, complicates our ability

363 to predict aspects of the ice age as they relate to biological productivity and diversity (*cf.* Olcott et al.,  
364 2005; Corsetti et al., 2006).

365

### 366 *5.3 The Vazante Group in the context of a late Mesoproterozoic world*

367 The upper part of the Vazante Group (as originally described by Dardenne, 2000) is thus far the  
368 only radiometrically constrained Mesoproterozoic succession preserving lithological and geochemical  
369 evidence of glaciation, so caution about its global significance is warranted. Other studies of late  
370 Mesoproterozoic strata indicate that this was a period of a global greenhouse conditions marked by  
371 eustatic highstand (Kah et al., 1999; 2012; Gilleaudeau and Kah, 2013). This conundrum may be  
372 explained by one of three scenarios: 1) the diamictites of the upper section of the Vazante Group have  
373 been mis-identified as glaciogenic; 2) the Re-Os system has been perturbed or mis-interpreted, and the  
374 apparent isochron ages do not reflect the timing of deposition; or 3) the Vazante Group accurately  
375 captures a previously unobserved component of the late Mesoproterozoic Earth.

376 There is strong evidence that units within these strata are the result of multiple discrete glacial  
377 events. Glaciation is the most likely mechanism that unites the geology (faceted and striated dropstones  
378 along with iron-formation), mineralogy (glendonite) and geochemistry (negative  $\delta^{13}\text{C}$  excursions) of the  
379 upper Vazante Group diamictites. Citing these lines of evidence, this study is not the first to have  
380 interpreted glacial strata within the Vazante Group (*cf.* Dardenne, 2001; Azmy et al., 2001; Brody et al.,  
381 2004; Olcott et al., 2005; Azmy et al., 2006; Misi et al., 2007). However, the Vazante Group diamictites  
382 have commonly been interpreted as correlative with Neoproterozoic “snowball Earth” deposits found atop  
383 the São Francisco craton (Misi et al., 2005) and the conjugate Congo craton (Azmy et al., 2001; 2006). If  
384 the Re-Os ages are correct, these correlations will need to be revised. These new data do not warrant  
385 altering the interpretation of glacial episodes within the Vazante Group, merely their timing.

386 The Re-Os system in organic-rich shale has been shown to be fairly robust. It appears  
387 unperturbed by low-grade metamorphism (Kendall et al., 2004) and hydrocarbon maturation and  
388 expulsion (Creaser et al., 2002) but can be disturbed by surface weathering (Jaffe et al., 2002). The

389 Vazante Group has been exposed to only sub-greenschist facies metamorphism (Babinski et al., 2005;  
390 Azmy et al., 2008) in the outcrop region. Furthermore, we sampled from unweathered and well-preserved  
391 cores (Azmy et al., 2006). While it is possible for detrital components of the shale to contaminate the  
392 hydrogenous Re-Os signatures and thereby influence the isochron ages, we used the Cr<sup>VI</sup>-H<sub>2</sub>SO<sub>4</sub> digestion  
393 medium that preferentially attacks the hydrogenous component of the shale over detrital input (Selby and  
394 Creaser, 2003; Kendall et al., 2004). Hydrothermal fluid flow can disturb Re-Os systematics but  
395 documented cases of remobilization of Re and Os under such conditions have resulted in erroneously  
396 *younger*, not older, ages (Kendall et al., 2009). Therefore, even with hydrothermal perturbation, the Serra  
397 do Garrote and Morro do Calcário glaciations would not be correlative with the younger, globally  
398 distributed Neoproterozoic events.

399         If the detrital input includes organic matter – as suggested for the post-glacial shale of the Morro  
400 do Calcário Formation (Marshall et al., 2009) – then preferential digestion of hydrogenous components  
401 may result in mixing of authigenic and detrital components and complicated Re-Os systematics. It seems  
402 unlikely, however, that such a mixing process would have a consistently wide-spread impact (both  
403 temporally and spatially) and result in isochronous relationships. Moreover, the Vazante *stata* Re-Os  
404 dates presented here are in stratigraphic agreement with one another, over a time scale of hundreds of  
405 millions of years, and derived from cores drilled approximately three kilometers apart. Furthermore,  
406 while the Morro do Calcário shale is clearly related to glacial phenomenon, the Serra do Garrote shale is  
407 not and thus detrital organic matter contamination through weathering inputs (*cf.* Johnston et al., 2012)  
408 should be considerably less significant.

409         The abundance and wide geographic spread of open marine and epicratonic carbonate platform  
410 deposits from the Mesoproterozoic, including the Bangemall Group (Buick et al., 1995), the Turukhansk  
411 Group (Knoll et al., 1995; Bartley et al., 2001), the Society Cliffs Formation (Kah et al., 2001) and the  
412 Atar Group (Kah et al., 2012) support the view of a world with globally high sea levels. Notably, the  
413 carbon isotope records of these successions are characterized by relatively little variation, predominantly  
414 ranging between -4‰ and +4‰, with shifts generally not exceeding 5‰ (Kah et al., 1999; Bartley et al.,

415 2001; Bartley et al., 2007; Kah et al., 2012; Gilleaudeau and Kah, 2013). This record stands in stark  
416 contrast to the succeeding Neoproterozoic when carbon isotope compositions of marine proxies reveal  
417 significant overall  $^{13}\text{C}$  enrichments and high amplitude variations (Knoll et al., 1986; Kaufman and Knoll,  
418 1995; Kaufman et al., 1997; Prave et al., 2009; Halverson et al., 2010).

419 As mentioned above, carbon isotope compositions of marine carbonates in the Vazante Group  
420 reveal a moderate spread in  $\delta^{13}\text{C}$  values, largely falling within the range of -4‰ to +3‰ (Azmy et al.,  
421 2006). This range is consistent with other late Mesoproterozoic successions lacking evidence for  
422 glaciation (e.g. Kah et al., 1999). Stratigraphically coherent negative carbon isotope excursions in these  
423 successions have recently been explained as a result of relative sea level highstands, which promote  
424 anoxia and organic matter remineralization in epicratonic environment (Gilleaudeau and Kah, 2013). In  
425 contrast, the upper Vazante Group displays two consistent basin-wide negative shifts of up to 8‰  
426 immediately above the interpreted glacial units (Azmy et al., 2006). Furthermore, the positive S isotope  
427 excursion captured in the lower Morro do Calcário shale, which occurs over just 20 meters of section  
428 (Fig. 6) is similar in magnitude to an event recorded from late Mesoproterozoic bedded sulfates on Baffin  
429 Island (Kah et al., 2004). This biogeochemical anomaly is best explained as the result of widespread  
430 removal of sulfate (via bacterial sulfate reduction) from an ocean that was relatively sulfate-poor  
431 (Canfield, 1998; Kah et al., 2004).

432 Given the uncertainties of the Re-Os ages presented here and previously (Azmy et al., 2008) and  
433 lack of geochronometric constraints in most other late Mesoproterozoic basins, it seems possible that the  
434 interval was environmentally variable or that there was a strong temperature gradient between the poles  
435 and equator. Paleomagnetic reconstructions place the São Francisco craton at high southern latitudes (45  
436 to over 60° S) in the late Mesoproterozoic (Weil et al., 1998; Tohver et al., 2006), allowing the possibility  
437 that the glaciations of the Morro do Calcário and Serra do Garrote formations were local rather than  
438 global in extent.

439 Re-Os age estimates from the Tourist and En Nesoar formations of the Atar Group are  
440 statistically identical to the Morro do Calcário Formation (~1100 Ma; Rooney et al., 2010). The

441 similarity of these ages (and  $Os_i$  values) as well as their carbon isotopic records have led to the suggestion  
442 that these units were deposited coevally atop the West African and São Francisco cratons, respectively  
443 (Rooney et al., 2010). Although some aspects of the geochemistry and radiometric constraints are  
444 consistent with this hypothesis, the two successions were clearly deposited under conflicting climatic  
445 conditions causing other researchers (Kah et al., 2012) to question this correlation. Alternatively, the  
446 imprecise age for the Morro do Calcário (Azmy et al., 2008) allow the possibility that Vazante  
447 glaciogenic units are younger than the Tourist and En Nesoar formations of the Atar Group. Given the  
448 incision of the glacial units into the underlying carbonate platforms (Fig. 2), the Morro do Calcário and  
449 Lapa formations may document more substantial sea-level falls following Mesoproterozoic highstands  
450 captured elsewhere. Lacking a wider range of sedimentary units from this time period for comparison, it  
451 may not be possible to reconcile the Atar Group and other contemporary basins with the Vazante Group  
452 until more precise age constraints are available.

453

## 454 **6. Conclusions**

455 Based on our geological and radiometric study of Vazante Group strata in south-central Brazil,  
456 we conclude that the upper 2/3 of the succession was deposited on a passive margin of the São Francisco  
457 craton during the late Mesoproterozoic Era. The Re-Os radiometric ages for the Serra do Garrote ( $1345 \pm$   
458  $88$  Ma; this study) and Morro do Calcário ( $1100 \pm 77$  Ma; Azmy et al., 2008) are consistent with previous  
459 estimates for upper Vazante strata based on the U-Pb age distributions of detrital zircons. Paleontological  
460 and carbon isotopic constraints also support a correlation of the upper section of the Vazante Group  
461 (above the Lagamar fault) with the Paranoá Group (also atop the São Francisco Craton), but not the  
462 Neoproterozoic Bambuí Group as suggested by earlier authors.

463 Evidence of two discrete glacial episodes in the upper part of the Vazante stratigraphy is  
464 preserved as 1) discrete diamictite horizons bearing both angular and rounded, faceted and striated clasts,  
465 sometimes preserved as dropstones in laminated shale; 2) the presence of the cold-water carbonate

466 mineral glendonite within one of the post-glacial shale horizons; 3) Fe-oxide cementation and local  
467 accumulation of iron-formation; and 4) negative  $\delta^{13}\text{C}$  excursion in carbonate overlying the diamictites.

468         Furthermore, we have identified map and field evidence for an oblique-slip reverse fault that  
469 juxtaposes Neoproterozoic glaciogenic strata of the lower Vazante Group (Rocinha and St. Antônio do  
470 Bonito) beneath late Mesoproterozoic formations of the upper Vazante Group, including the Serra do  
471 Garrote, Morro do Calcário and Lapa units evaluated in this geochemical study. While the fault solves  
472 the paradoxical U-Pb maximum depositional ages derived from detrital zircons and the stratigraphic  
473 inversion, it also opens up the possibility of other, yet undiscovered, faults within the sequence which  
474 may further complicate stratigraphic relationships.

475         The Vazante Group is unique in the late Mesoproterozoic in that it displays evidence of glaciation  
476 in a period generally regarded as a time of greenhouse conditions and globally high sea levels. The  
477 glaciations may be regional phenomena as paleo-reconstructions place the São Francisco craton at high  
478 southern latitudes during the late Mesoproterozoic Era, but the general lack of open marine successions  
479 from this time interval limits our current understanding of this ancient episode of Earth history.

480

#### 481 **Acknowledgments**

482         The authors wish to thank Kristina Bartlett Brody and Natalie Sievers at the University of  
483 Maryland for assistance with analyses and Julio Pinho for help in the field. We also thank Votorantim  
484 Metais for access to the drill core samples. This work was partly funded by the National Science  
485 Foundation and the Natural Research Council of Brazil. Comments from Ruth Schulte and Jim Coleman  
486 of the USGS, Julie Bartley, Linda Kah and Geoff Gilleaudeau, as well as two anonymous reviewers  
487 appointed by the journal greatly improved this paper. Any use of trade, firm, or product names is for  
488 descriptive purposes only and does not imply endorsement by the U.S. Government.

489

#### 490 **References Cited**

491 Amaral, G., Kawashita, K., 1967. Determinacao da idade do Grupo Bambui pelo metodo Rb/Sr. Anais  
492 21st Congresso Brasileiro Geologia Curitiba, Brasil, pp. 214-217.

493 Anbar, A.D., Duan, Y., Lyons, T.W., Arnold, G.L., Kendall, B., Creaser, R.A., Kaufman, A.J., Gordon,  
494 G.W., Scott, C., Garvin, J., Buick, R., 2007. A whiff of oxygen before the Great Oxidation  
495 Event? Science 317, 1903-1906.

496 Azmy, K., Kaufman, A.J., Misi, A., de Oliveira, T.F., 2006. Isotope stratigraphy of the Lapa Formation,  
497 São Francisco Basin, Brazil: Implications for Late Neoproterozoic glacial events in South  
498 America. Precambrian Res 149, 231-248.

499 Azmy, K., Kendall, B., Creaser, R.A., Heaman, L., de Oliveira, T.F., 2008. Global correlation of the  
500 Vazante Group, São Francisco Basin, Brazil: Re-Os and U-Pb radiometric age constraints.  
501 Precambrian Res 164, 160-172.

502 Azmy, K., Veizer, J., Misi, A., de Oliveira, T.F., Sanches, A.L., Dardenne, M.A., 2001. Dolomitization  
503 and isotope stratigraphy of the Vazante Formation, Sao Francisco Basin, Brazil. Precambrian  
504 Res 112, 303-329.

505 Babinski, M., Monteiro, L.S., Fetter, A.H., Bettencourt, J.S., Oliveira, T.F., 2005. Isotope geochemistry  
506 of the mafic dikes from the Vazante nonsulfide zinc deposit, Brazil. J S Am Earth Sci 18, 293-  
507 304.

508 Babinski, M., Vieira, L.C., Trindade, R.I.F., 2007. Direct dating of the Sete Lagoas cap carbonate  
509 (Bambuí Group, Brazil) and implications for the Neoproterozoic glacial events. Terra Nova 19,  
510 401-406.

511 Bartley, J.K., Kah, L.C., McWilliams, J.L., Stagner, A.F., 2007. Carbon isotope chemostratigraphy of the  
512 Middle Riphean type section (Avzyan Formation, Southern Urals, Russia): Signal recovery in a  
513 fold-and-thrust belt. Chem Geol 237, 211-232.

514 Bartley, J.K., Semikhatov, M.A., Kaufman, A.J., Knoll, A.H., Pope, M.C., Jacobsen, S.B., 2001. Global  
515 events across the Mesoproterozoic-Neoproterozoic boundary: C and Sr isotopic evidence from  
516 Siberia. Precambrian Res 111, 165-202.

517 Bekker, A., Kaufman, A.J., Karhu, J.A., Eriksson, K.A., 2005. Evidence for Paleoproterozoic cap  
518 carbonates in North America. *Precambrian Research* 137, 167-206.

519 Birck, J.L, Roy Barman, M., Capmas, F., 1997. Re-Os isotopic measurements at the femtomole level in  
520 natural samples. *Geostandards Newsletter* 21, 19-27.

521 Brody, K.B., Kaufman, A.J., Eigenbrode, J.L., Cody, G.D., 2004. Biomarker geochemistry of a post-  
522 glacial Neoproterozoic succession in Brazil, Geological Society of America Annual Meeting  
523 (Abstract), Denver, CO.

524 Buick, R., Marais, D.J.D., Knoll, A.H., 1995. Stable Isotopic Compositions of Carbonates from the  
525 Mesoproterozoic Bangemall Group, Northwestern Australia. *Chem Geol* 123, 153-171.

526 Canfield, D.E., 1998. A new model for Proterozoic ocean chemistry. *Nature* 396, 450-453.

527 Canfield, D.E., Raiswell, R., Westrich, J.T., Reaves, C.M., Berner, R.A., 1986. The Use of Chromium  
528 Reduction in the Analysis of Reduced Inorganic Sulfur in Sediments and Shales. *Chem Geol* 54,  
529 149-155.

530 Canfield, D.E., Raiswell, R., Bottrell, S., 1992. The reactivity of sedimentary iron minerals toward  
531 sulfide. *Am J Sci* 292, 659-683.

532 Cloud, P., Dardenne, M.A., 1973. Proterozoic age of the Bambui Group in Brazil. *Geol Soc Am Bull* 84,  
533 1673-1676.

534 Cohen, A.S., Coe, A.L., Bartlett, J.M., Hawkesworth, C.J., 1999. Precise Re-Os ages of organic-rich  
535 mudrocks and the Os isotope composition of Jurassic seawater. *Earth Planet Sc Lett* 167, 159-  
536 173.

537 Cohen, A.S., Waters, F.G., 1996. Separation of osmium from geological materials by solvent extraction  
538 for analysis by thermal ionization mass spectrometry. *Analytica Chimica Acta* 332, 269-275.

539 Corsetti, F.A., Olcott, A.N., Bakermans, C., 2006. The biotic response to Neoproterozoic snowball Earth.  
540 *Palaeogeogr Palaeoclimatol Palaeoecol* 232, 114-130.

541 Creaser, R.A., Sannigrahi, P., Chacko, T., Selby, D., 2002. Further evaluation of the Re-Os  
542 geochronometer in organic-rich sedimentary rocks: A test of hydrocarbon maturation effects in

543 the Exshaw Formation, Western Canada Sedimentary Basin. *Geochim Cosmochim Acta* 66, 3441-  
544 3452.

545 Dardenne, M.A., 1978. Zonação tectônica na borda ocidental do Cráton São Francisco. *Anais Congresso*  
546 *Brasileiro de Geologia, Sociedade Brasileira de Geologia, Recife, v. 1, pp. 299-308.*

547 Dardenne, M.A., 2000. The Brasilia Fold Belt, in: Cordani, U.G., Milani, E.J., Filho, A.T., Campos, D.A.  
548 (Eds.), *The Brasilia Fold Belt in Tectonic Evolution of South America. 31st International*  
549 *Geological Congress, Rio de Janeiro, pp. 231-263.*

550 Dardenne, M.A., 2001. Lithostratigraphic sedimentary sequences of the Vazante Group, in: IGCP 450  
551 *Proterozoic Sediment-Hosted Base Metal Deposits of Western Gondwana (abstract), Belo*  
552 *Horizonte, pp. 48-50.*

553 Dardenne, M.A., Campos Neto, M.C., 1976. Geologia da região de Lagamar, Minas Gerais, Congresso  
554 *Brasileiro de Geologia, 29, Ouro Preto, resumos, pp. 17.*

555 Derry, L.A., Kaufman, A.J., Jacobsen, S.B., 1992. Sedimentary cycling and environmental-change in the  
556 *Late Proterozoic - evidence from stable and radiogenic isotopes. Geochim Cosmochim Acta* 56,  
557 1317-1329.

558 Gilleaudeau, G.J., Kah, L.C. (2013) Carbon isotope records in a Mesoproterozoic epicratonic sea: Carbon  
559 cycling in a low-oxygen world. *Precambrian Res* 228, 85-101.

560 Halverson, G.P., Wade, B.P., Hurtgen, M.T., Barovich, K.M., 2010. Neoproterozoic chemostratigraphy.  
561 *Precambrian Res* 182, 337-350.

562 Hannah, J.L., Bekker, A., Stein, H.J., Markey, R.J., Holland, H.D., 2004. Primitive Os and 2316 Ma age  
563 for marine shale: implications for Paleoproterozoic glacial events and the rise of atmospheric  
564 oxygen. *Earth Planet Sc Lett* 225, 43-52.

565 Harland, W.B., and Bidgood, D.E.T., 1959. Palaeomagnetism in some Norwegian sparagmites and the  
566 late Pre-Cambrian ice age. *Nature* 184, 1860-1862.

567 Hoffman, P.F., Kaufman, A.J., Halverson, G.P., Schrag, D.P., 1998. A Neoproterozoic snowball earth.  
568 *Science* 281, 1342-1346.

569 Jaffe, L.A., Peucker-Ehrenbrink, B., Petsch, S.T., 2002. Mobility of rhenium, platinum group elements  
570 and organic carbon during black shale weathering. *Earth Planet Sc Lett* 198, 339-353.

571 Johnston, D.T., Macdonald, F.A., Gill, B.C., Hoffman, P.F., and Schrag, D.P., 2012. Uncovering the  
572 Neoproterozoic carbon cycle. *Nature* 483, 320-324.

573 Kah, L.C., Bartley, J.K., Teal, D.A., 2012. Chemostratigraphy of the Late Mesoproterozoic Atar Group,  
574 Taoudeni Basin, Mauritania: Muted isotopic variability, facies correlation, and global isotopic  
575 trends. *Precambrian Res* 200, 82-103.

576 Kah, L.C., Lyons, T.W., Chesley, J.T., 2001. Geochemistry of a 1.2 Ga carbonate-evaporite succession,  
577 northern Baffin and Bylot Islands: implications for Mesoproterozoic marine evolution.  
578 *Precambrian Res* 111, 203-234.

579 Kah, L.C., Lyons, T.W., Frank, T.D., 2004. Low marine sulphate and protracted oxygenation of the  
580 proterozoic biosphere. *Nature* 431, 834-838.

581 Kah, L.C., Sherman, A.G., Narbonne, G.M., Knoll, A.H., Kaufman, A.J., 1999.  $\delta^{13}\text{C}$  stratigraphy of  
582 the Proterozoic Bylot Supergroup, Baffin Island, Canada: implications for regional  
583 lithostratigraphic correlations. *Can J Earth Sci* 36, 313-332.

584 Kaufman, A.J., Hayes, J.M., Knoll, A.H., Germs, G.J.B., 1991. Isotopic compositions of carbonates and  
585 organic-carbon from upper Proterozoic successions in Namibia-Stratigraphic variation and the  
586 effects of diagenesis and metamorphism. *Precambrian Res* 49, 301-327.

587 Kaufman, A.J., Knoll, A.H., 1995. Neoproterozoic Variations in the C-Isotopic Composition of Seawater  
588 - Stratigraphic and Biogeochemical Implications. *Precambrian Res* 73, 27-49.

589 Kaufman, A.J., Knoll, A.H., Narbonne, G.M., 1997. Isotopes, ice ages, and terminal Proterozoic earth  
590 history. *P Natl Acad Sci USA* 94, 6600-6605.

591 Kendall, B., Creaser, R.A., Selby, D., 2006. Re-Os geochronology of postglacial black shales in  
592 Australia: Constraints on the timing of "Sturtian" glaciation. *Geology* 34, 729-732.

593 Kendall, B., Creaser, R.A., Ross, G.M., Selby, D., 2004. Constraints on the timing of Marinoan  
594 "Snowball Earth" glaciation by Re-187-Os-187 dating of a Neoproterozoic, post-glacial black  
595 shale in Western Canada. *Earth Planet Sc Lett* 222, 729-740.

596 Kendall, B., Creaser, R.A., Gordon, G.W., Anbar, A.D., 2009. Re-Os and Mo isotope systematics of  
597 black shales from the Middle Proterozoic Velkerri and Wollongorang Formations, McArthur  
598 Basin, northern Australia. *Geochim Cosmochim Ac* 73, 2534-2558.

599 Kennedy, M.J., 1996. Stratigraphy, sedimentology, and isotopic geochemistry of Australian  
600 Neoproterozoic postglacial cap dolostones: Deglaciation, delta C-13 excursions, and carbonate  
601 precipitation. *Journal of Sedimentary Research* 66, 1050-1064.

602 Kennedy, M.J., Runnegar, B., Prave, A.R., Hoffmann, K.H., Arthur, M.A., 1998. Two or four  
603 Neoproterozoic glaciations? *Geology* 26, 1059-1063.

604 Kirschvink, J.W., 1992. Late Proterozoic low-latitude global glaciations: the Snowball Earth, in: Schopf,  
605 J.W., Klein, C. (Eds.), *The Proterozoic Biosphere*. Cambridge University Press, Cambridge, pp.  
606 51-52.

607 Knoll, A.H., Hayes, J.M., Kaufman, A.J., Swett, K., Lambert, I.B., 1986. Secular Variation in Carbon  
608 Isotope Ratios from Upper Proterozoic Successions of Svalbard and East Greenland. *Nature* 321,  
609 832-838.

610 Knoll, A.H., Kaufman, A.J., Semikhatov, M.A., 1995. The carbon-isotopic composition of Proterozoic  
611 carbonates: Riphean successions from northwestern Siberia (Anabar Massif, Turukhansk uplift).  
612 *Am J Sci* 295, 823-850.

613 Levasseur, S., Birck, J.-L., Allègre, C.J., 1999. The osmium riverine flux and the oceanic mass balance of  
614 osmium. *Earth Planet Sci Lett* 174, 7-23.

615 Marshall, A.O., Corsetti, F.A., Sessions, A.L., Marshall, C.P., 2009. Raman spectroscopy and biomarker  
616 analysis reveal multiple carbon inputs to a Precambrian glacial sediment. *Organic Geochemistry*  
617 40, 1115-1123.

618 Misi, A., Azmy, K., Kaufman, A.J., Oliveira, T.F., Pinho, J.M., Sanches, A.L., 2010. Metallogenic and  
619 phosphogenic events in the intracratonic and passive-margin Proterozoic basins of the São  
620 Francisco Craton: The Bambuí/Una and Vazante Groups. VII South American Symposium on  
621 Isotope Geology, Brasilia, DF. Extended Abstracts.

622 Misi, A., Azmy, K., Kaufman, A.J., Oiveira, T. F., Pinho, J. M., Sanches, A.L., 2011. High resolution  
623 chemostratigraphy and Re-Os ages of organic shales of the Vazante Group (Minas Gerais,  
624 Brazil): Implications for mineral exploration modelling. In: XIV Congreso Latino Americano de  
625 Geologia, Medellin. Memorias, v. 1. p. 410-411.

626 Misi, A., Iyer, S.S.S., Coelho, C.E.S., Tassinari, C.C.G., Franca-Rocha, W.J.S., Cunha, I.D., Gomes,  
627 A.S.R., de Oliveira, T.F., Teixeira, J.B.G., Filho, V.M.C., 2005. Sediment hosted lead-zinc  
628 deposits of the Neoproterozoic Bambui Group and correlative sequences, Sao Francisco Craton,  
629 Brazil: A review and a possible metallogenic evolution model. *Ore Geol Rev* 26, 263-304.

630 Misi, A., Kaufman, A.J., Veizer, J., Powis, K., Azmy, K., Boggiani, P.C., Gaucher, C., Teixeira, J.B.G.,  
631 Sanches, A.L., Iyer, S.S.S., 2007. Chemostratigraphic correlation of neoproterozoic successions  
632 in South America. *Chem Geol* 237, 143-167.

633 Olcott, A.N., Sessions, A.L., Corsetti, F.A., Kaufman, A.J., de Oliviera, T.F., 2005. Biomarker evidence  
634 for photosynthesis during Neoproterozoic glaciation. *Science* 310, 471-474.

635 Pimentel, M.M., Dardenne, M.A., Fuck, R.A., Viana, M.G., Junges, S.L., Fischel, D.P., Seer, H.J.,  
636 Dantas, E.L., 2001. Nd isotopes and the provenance of detrital sediments of the Neoproterozoic  
637 Brasilia Belt, central Brazil. *J S Am Earth Sci* 14, 571-585.

638 Pinho, J.M.M., Dardenne, M.A., 1994. Caracterização da Falha de Lagamar, NW de Minas Gerais.  
639 Abstracts, 38th Brazilian Geological Congress, Sociedade Brasileira de Geologia, Camboriú, SC  
640 p.246-247.

641 Poulton, S.W., Canfield, D.E., 2005. Development of a sequential extraction procedure for iron:  
642 implications for iron partitioning in continentally derived particulates. *Chem Geol* 214, 209-221.

643 Poulton, S.W., Raiswell, R., 2002. The low-temperature geochemical cycle of iron: From continental  
644 fluxes to marine sediment deposition. *Am J Sci* 302, 774-805.

645 Poulton, S.W., Canfield, D.E., 2011. Ferruginous conditions: A dominant feature of the ocean through  
646 Earth's history. *Elements* 7, 107-112.

647 Poulton, S.W., Krom, M.D., Raiswell, R., 2004a. A revised scheme for the reactivity of iron  
648 (oxyhydr)oxide minerals towards dissolved sulfide. *Geochim Cosmochim Acta* 68, 3703-3715.

649 Poulton, S.W., Fralick, P.W., Canfield, D.E., 2004b. The transition to a sulphidic ocean ~1.84 billion  
650 years ago. *Nature* 431, 173-177.

651 Prave, A.R., Fallick, A.E., Thomas, C.W., Graham, C.M., 2009. A composite C-isotope profile for the  
652 Neoproterozoic Dalradian Supergroup of Scotland and Ireland. *J Geol Soc London* 166, 845-  
653 857.

654 Raiswell, R. Canfield, D.E., 1998. Sources of iron for pyrite formation in modern sediments. *Am J Sci*  
655 298, 219-245.

656 Ravizza, G., Turekian, K.K., 1989. Application of the Re-187-Os-187 System to Black Shale  
657 Geochronometry. *Geochimica Et Cosmochimica Acta* 53, 3257-3262.

658 Rodrigues, J.B., Pimentel, M.M., Buhn, B., Matteini, M., Dardenne, M.A., Alvarenga, C.J.S., Armstrong,  
659 R.A., 2012. Provenance of the Vazante Group: New U-Pb, Sm-Nd, Lu-Hf isotopic data and  
660 implications for the tectonic evolution of the Neoproterozoic Brasilia Belt. *Gondwana Res* 21,  
661 439-450.

662 Rooney, A.D., Selby, D., Houzay, J.P., Renne, P.R., 2010. Re-Os geochronology of a Mesoproterozoic  
663 sedimentary succession, Taoudeni basin, Mauritania: Implications for basin-wide correlations  
664 and Re-Os organic-rich sediments systematics. *Earth Planet Sc Lett* 289, 486-496.

665 Santos, R.V., de Alvarenga, C.J.S., Dardenne, M.A., Sial, A.N., Ferreira, V.P., 2000. Carbon and oxygen  
666 isotope profiles across Meso-Neoproterozoic limestones from central Brazil: Bambui and  
667 Paranoa groups. *Precambrian Res* 104, 107-122.

668 Schrag, D.P., Berner, R.A., Hoffman, P.F., and Halverson, G.P., 2002. On the initiation of a snowball  
669 Earth. *Geochemistry Geophysics Geosystems* 3, 6, 1-21.

670 Selby, D., Creaser, R.A., 2003. Re-Os geochronology of organic rich sediments: an evaluation of organic  
671 matter analysis methods. *Chem Geol* 200, 225-240.

672 Shirey, S.B., Walker, R.J., 1995. Carius Tube Digestion for Low-Blank Rhenium-Osmium Analysis. *Anal*  
673 *Chem* 67, 2136-2141.

674 Tohver, E., D'Agrella, M.S., Trindade, R.I.F., 2006. Paleomagnetic record of Africa and South America  
675 for the 1200-500 Ma interval, and evaluation of Rodinia and Gondwana assemblies.  
676 *Precambrian Res* 147, 193-222.

677 Walker, R.J., Horan, M.F., Morgan, J.W., Becker, H., Grossman, J.N., Rubin, A.E., 2002a. Comparative  
678  $^{187}\text{Re}$ - $^{187}\text{Os}$  systematics of chondrites: implications regarding early solar system processes.  
679 *Geochim Cosmochim Acta* 66, 4187-4201.

680 Walker, R.J., Prichard, H.M., Ishiwatari, A., Pimentel, M., 2002b. The osmium isotopic composition of  
681 the convecting upper mantle deduced from ophiolite chromites. *Geochim Cosmochim Acta* 66,  
682 329-345.

683 Walter, M.R., Veevers, J.J., Calver, C.R., Gorjan, P., Hill, A.C., 2000. Dating the 840-544 Ma  
684 Neoproterozoic interval by isotopes of strontium, carbon, and sulfur in seawater, and some  
685 interpretative models. *Precambrian Research* 100, 371-433.

686 Weil, A.B., Van der Voo, R., Mac Niocaill, C., Meert, J.G., 1998. The Proterozoic supercontinent  
687 Rodinia: paleomagnetically derived reconstructions for 1100 to 800 Ma. *Earth Planet Sc Lett*  
688 154, 13-24.

689

690 **Captions**

691 Figure 1: Geologic map of study area. The Vazante Group is elongated north to south within Brazil with  
692 † indicating the approximate location of the drill cores examined here. Modified from Babinski et al.  
693 (2005).

694  
695 Figure 2: Generalized stratigraphy of the Vazante Group with formation and member names highlighting  
696 sub-glacial valleys and post-glacial fill, the newly discovered reverse fault and geochronometric  
697 constraints discussed in the text. Modified after Dardenne (2000) with generalized C-isotope trends from  
698 Azmy et al. (2001; 2006). No vertical scale implied.

699  
700 Figure 3: Photographs of A. carbonate ice-rafted debris in the organic-rich post-glacial shale of the Morro  
701 do Calcário Formation in drill core MASW-01; B. faceted cobble in silicified shale matrix of the Morro  
702 do Calcário Formation near Paracatu, MG, Brazil; C. *Conophyton* stromatolites from the basal Lagamar  
703 Formation above the thrust fault; D. phosphorite and high-Sr limestone from the Rocinha Formation  
704 located below the thrust fault and west of the Vazante mine; E. thrust fault trace with brown to mauve  
705 sandy mylonite to the left and bedded purple shale and siltstone of the upper Rocinha Formation to the  
706 right; F. Close up of clay and quartz-rich mylonite at thrust fault contact.

707  
708 Figure 4: Re-Os isochrons for: A. Serra do Garrote Formation samples from drill core 134-86; B. Morro  
709 do Calcário Formation samples from drill core 42-88 and 134-86; C. Morro do Calcário Formation  
710 samples taken only from drill core 134-86.

711  
712 Figure 5: Time-series elemental and stable isotope compositions of the Serra do Garrote, Morro do  
713 Calcário and Lapa Formations (shale intervals only) in the Mesoproterozoic Vazante Group, drill core  
714 134-86 (data available in Table 2), where TOC = total organic carbon.

715

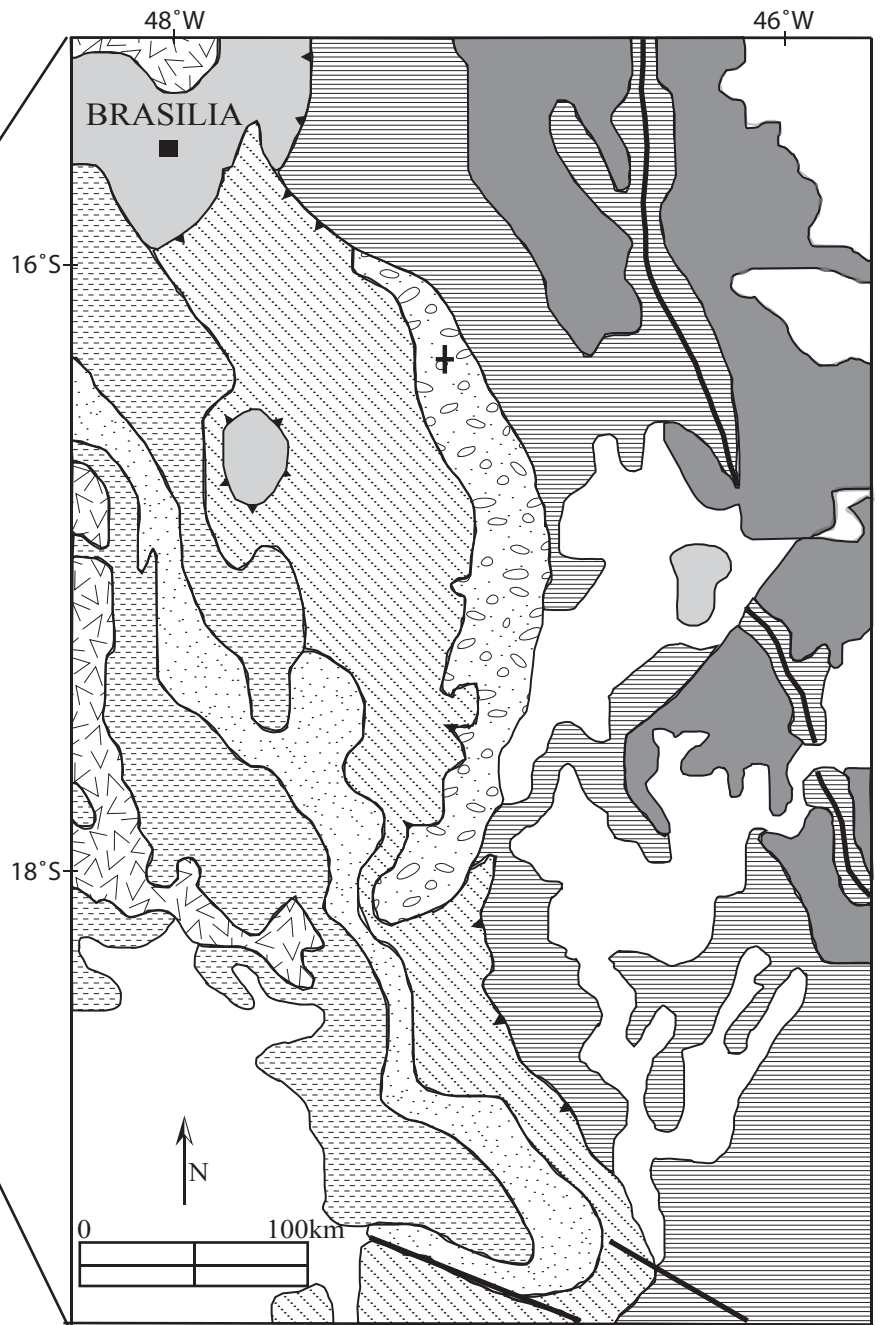
716 Figure 6: Time-series elemental and stable isotope compositions of the Morro do Calcário Formation  
717 shale interval in the Mesoproterozoic Vazante Group, drill core 42-88 (data available in Tables 2 and 3),  
718 where TOC = total organic carbon and S = sulfide-sulfur. Iron speciation data allows identification of  
719 deposition from an oxic, anoxic non-sulfidic or euxinic (free sulfide) water column. FeHR = highly  
720 reactive iron; FeT = total iron; FeS = pyrite iron. Euxinic conditions are interpreted from  $\text{FeHR}/\text{FeT} >$   
721  $0.38$  and  $\text{FeS}/\text{FeHR} > \sim 0.7$ ; anoxic non-sulfidic conditions are recognized from  $\text{FeHR}/\text{FeT} > 0.38$  and  
722  $\text{FeS}/\text{FeHR} < \sim 0.7$ ; oxic conditions are demonstrated by  $\text{FeHR}/\text{FeT} < 0.22$ . Dashed lines are presented at  
723 these threshold values. For all data points, the uncertainty on the measurement is smaller than the  
724 symbol.

725  
726 Table 1: Re and Os abundance and isotope data for black shale intervals in the Serra do Garrote, Morro do  
727 Calcário and Lapa Formations.  $\text{Os}_i$  = initial  $^{187}\text{Os}/^{188}\text{Os}$  ratio back-calculated using the isochron age in  
728 Figure 4.

729  
730 Table 2: Time-series total organic carbon (TOC) abundances in weight percent; carbon isotopic  
731 composition of the organic carbon ( $\delta^{13}\text{C}$ ); sulfur isotopic composition of the sulfide sulfur ( $\delta^{34}\text{S}$ ); and  
732 sulfide sulfur abundance in weight percent (S) of the Serra do Garrote, Morro do Calcário and Lapa  
733 Formations in drill core 134-86 as well as the Morro do Calcário Formation of drill core 42-88.  
734 Uncertainties do not exceed: TOC and S  $\pm 10\%$  of value;  $\delta^{13}\text{C} \pm 0.15\%$ ;  $\delta^{34}\text{S} \pm 0.35\%$ . nd = not  
735 detected.

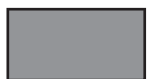
736  
737 Table 3: Results from the analysis of the Morro do Calcário Formation shale interval in the  
738 Mesoproterozoic Vazante Group, drill core 42-88. Iron speciation analyses: All concentrations are in  
739 weight % (nd = not detected). FeT = total iron; Fecarb = carbonate iron; Fox = oxide iron; Femag =  
740 magnetite iron; Fe-AVS = acid volatile sulfide iron; Fepy = pyrite iron; FeHR = highly reactive iron; Fe-S  
741 = Fe-AVS + Fepy.

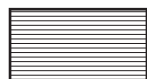
Fig. 1



 Phanerozoic Sediments

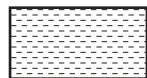
Bambuú Group

 Três Marias Fm.

 Paraopeba Subgroup

Brasília Fold Belt

 Ibíá Fm.

 Araxá Group

 Granulites

 Vazante Group

 Paranoá Group

 Canastra Group

Fig. 2

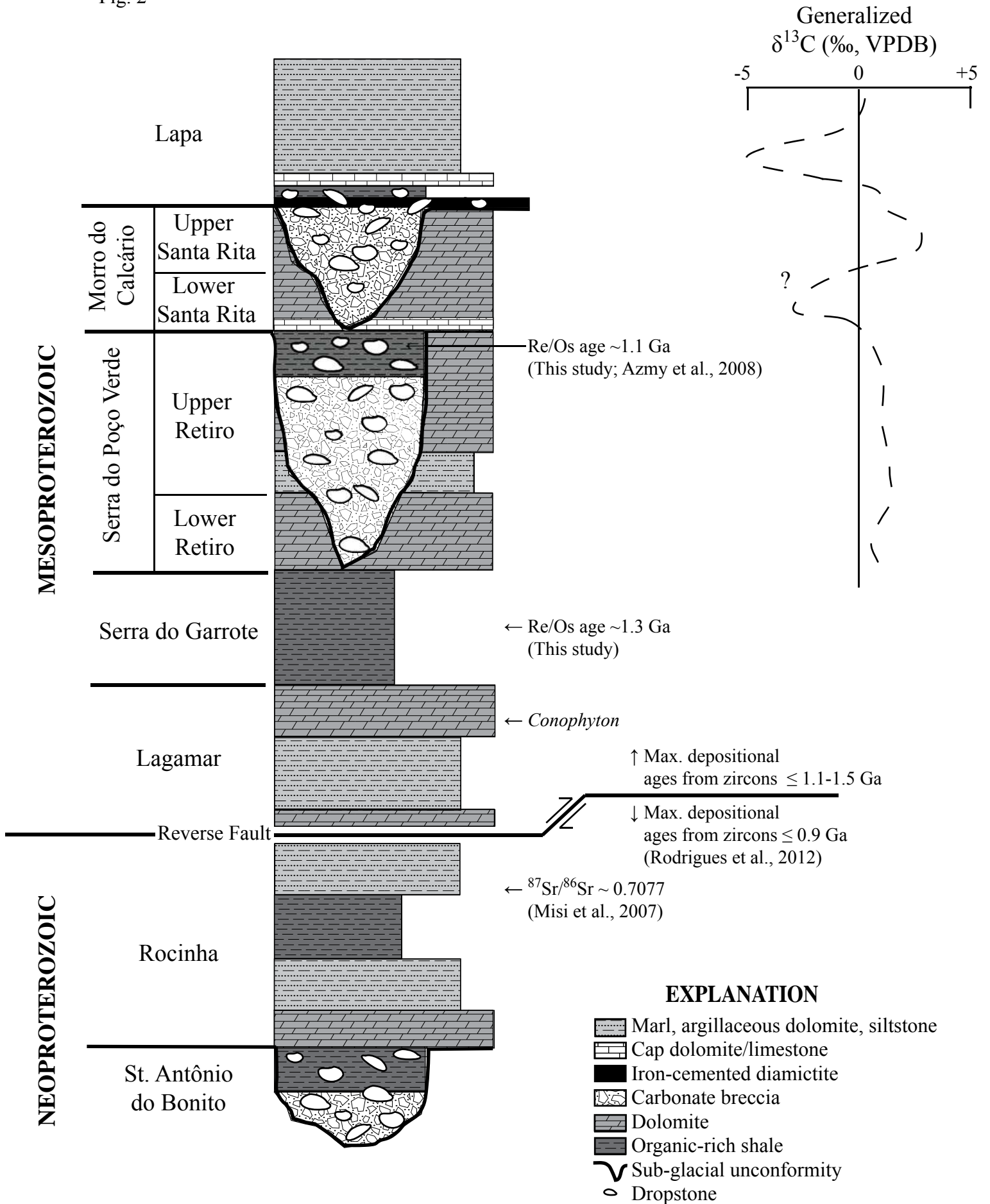
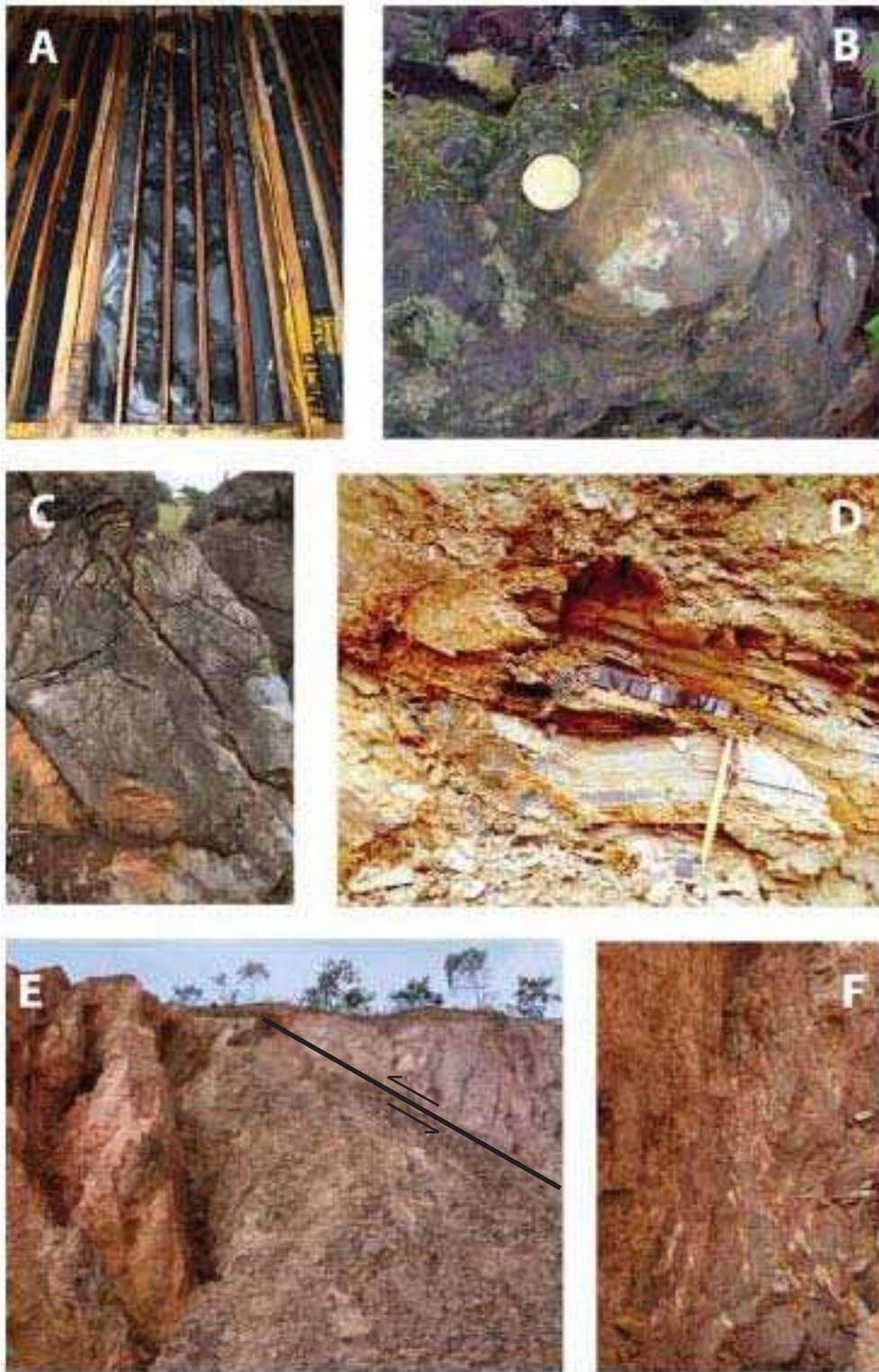


Fig. 3



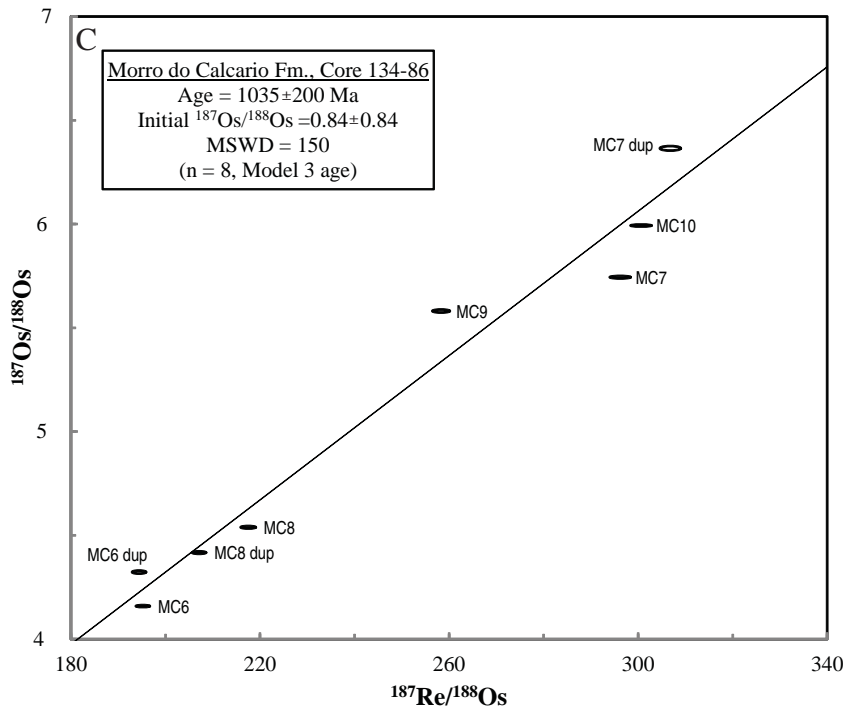
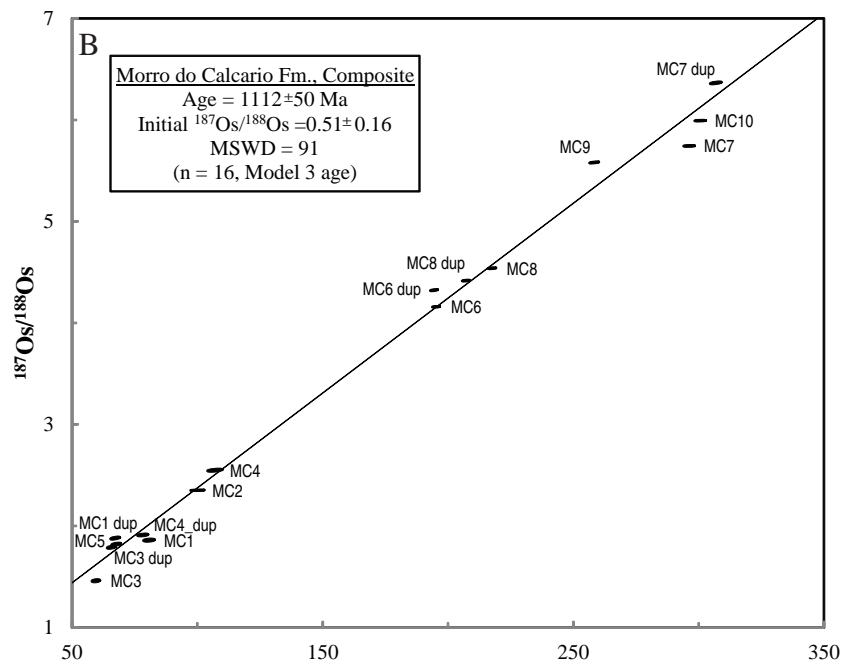
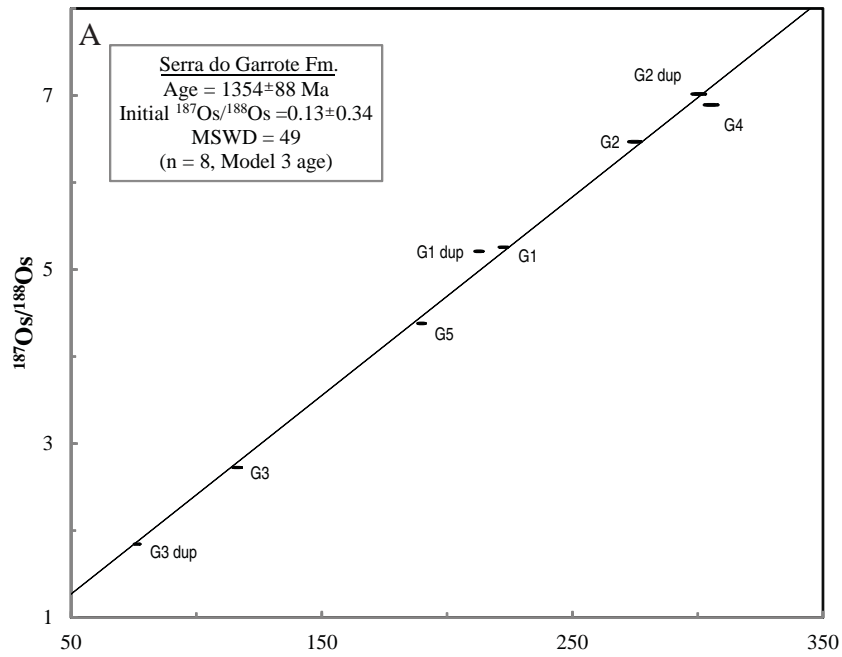


Fig. 5

Serra do Garrote, Morro do Calcário and Lapa Fm. Shale in Drillcore 134-86

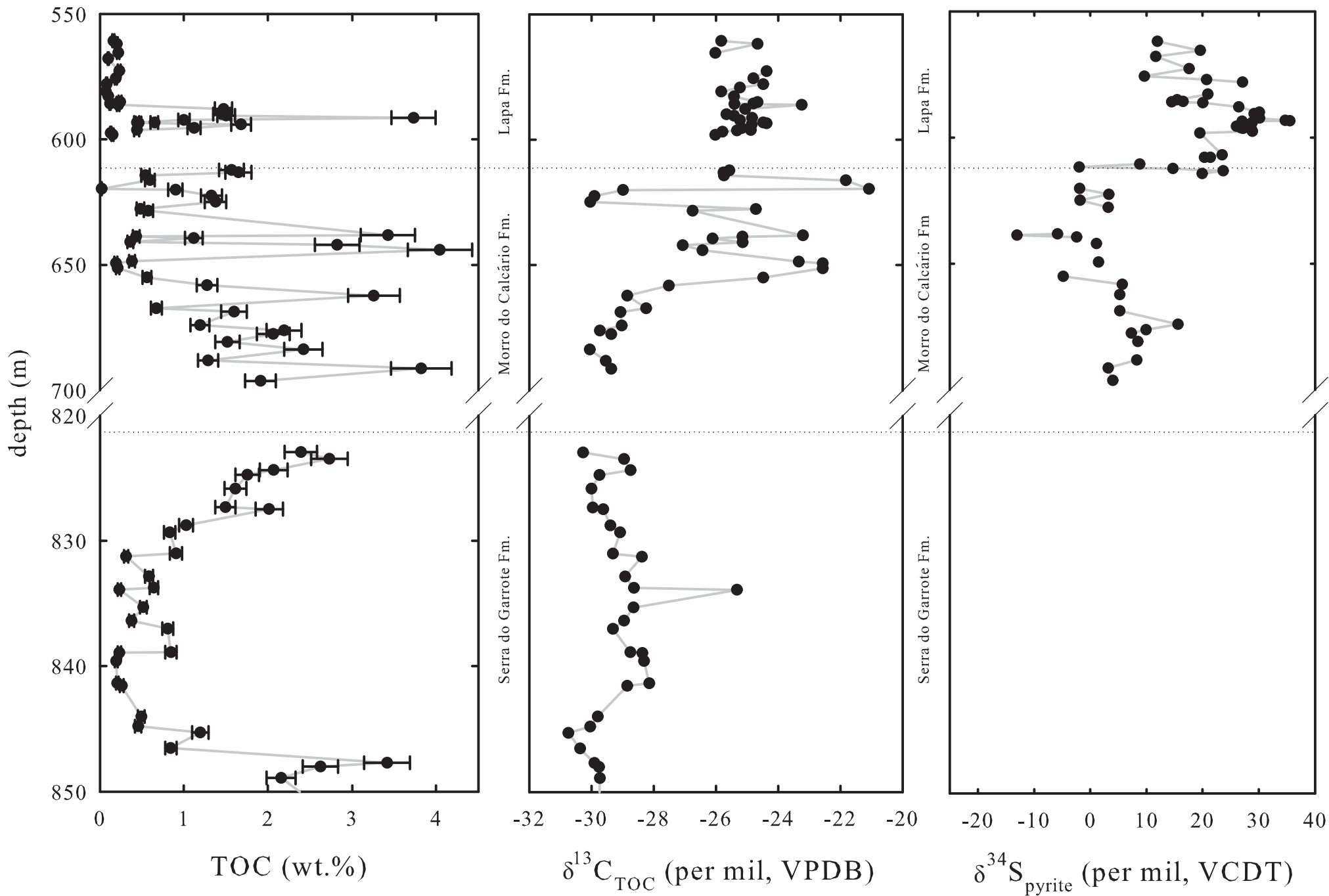


Fig. 6

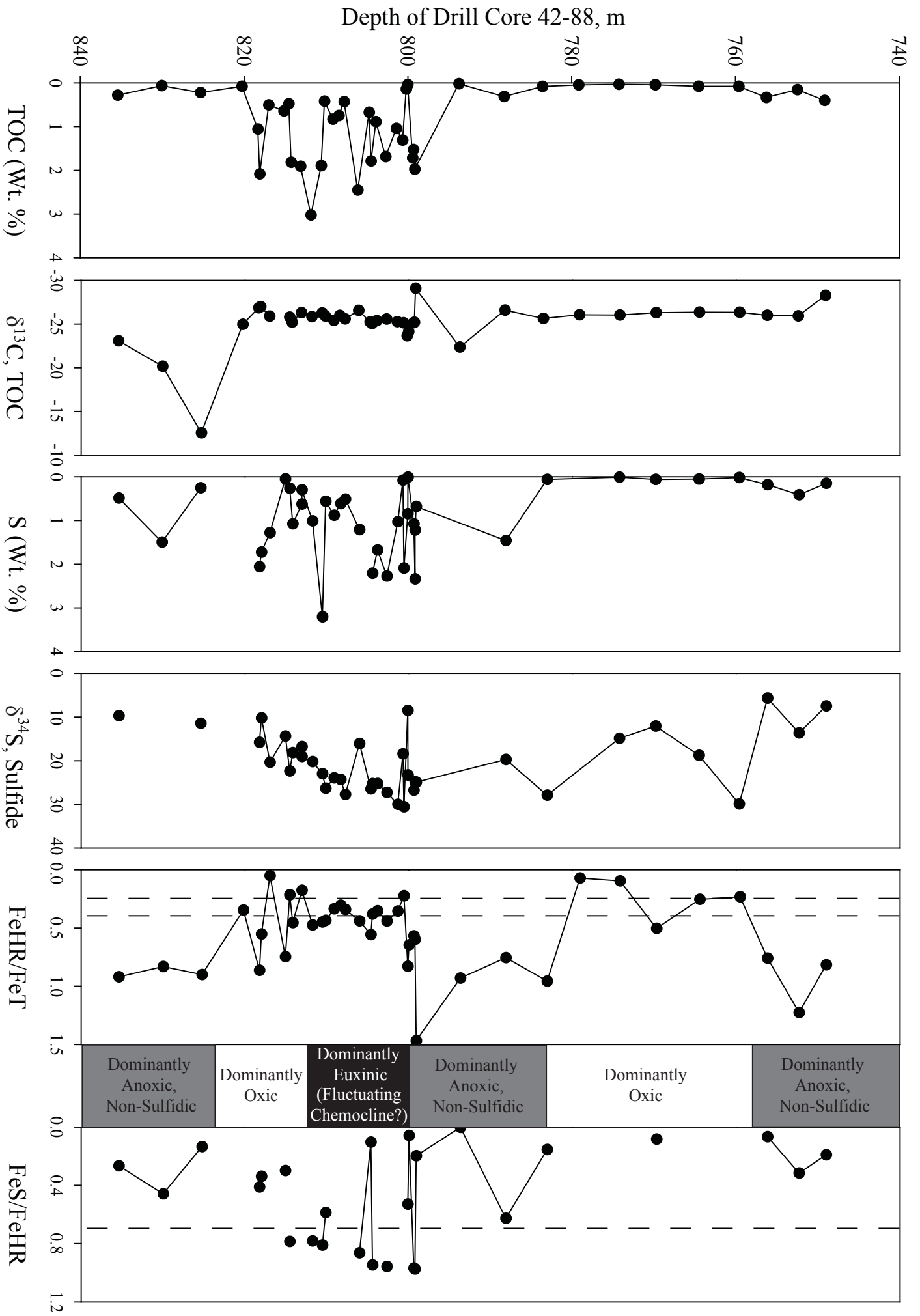


Table 1

	Sample	Drill Hole	Core Depth	Re (ppb)	Os (ppt)	$^{187}\text{Re} / ^{188}\text{Os}$	$^{187}\text{Os} / ^{188}\text{Os}$	Os <sub>i</sub>
Lapa Fm.	L1	134-86	587.84	0.322 ± 0.008	35.0 ± 0.4	53.34 ± 1.19	1.709 ± 0.003	N/A
	L2	134-86	589.90	0.288 ± 0.008	33.4 ± 0.4	50.73 ± 1.53	1.838 ± 0.007	N/A
	L3	134-86	590.50	0.138 ± 0.008	26.1 ± 0.4	30.4 ± 1.8	1.59 ± 0.01	N/A
	L4	134-86	591.34	0.366 ± 0.008	52.3 ± 0.5	39.05 ± 0.92	1.358 ± 0.006	N/A
Morro do Calcário Fm.	MC1	42-88	803.89	0.435 ± 0.009	31.6 ± 0.1	80.7 ± 1.8	1.86 ± 0.01	0.33
	MC1_dup	42-88	803.89	0.360 ± 0.007	31.5 ± 0.1	67.2 ± 1.5	1.88 ± 0.01	0.6
	MC2	42-88	804.00	0.690 ± 0.014	42.5 ± 0.1	100.0 ± 2.2	2.352 ± 0.003	0.46
	MC3	42-88	804.43	0.334 ± 0.007	31.6 ± 0.1	59.5 ± 1.3	1.46 ± 0.01	0.34
	MC3_dup	42-88	804.43	0.303 ± 0.006	26.9 ± 0.1	65.7 ± 1.4	1.79 ± 0.01	0.54
	MC4	42-88	804.48	0.858 ± 0.017	50.5 ± 0.2	107.0 ± 2.4	2.549 ± 0.01	0.53
	MC4_dup	42-88	804.48	0.831 ± 0.017	62.9 ± 0.2	78.2 ± 1.7	1.911 ± 0.009	0.44
	MC5	42-88	804.50	0.387 ± 0.008	33.5 ± 0.1	67.6 ± 1.5	1.82 ± 0.01	0.54
	MC6	134-86	676.05	3.498 ± 0.014	131.1 ± 0.4	195.2 ± 1.2	4.159 ± 0.004	0.46
	MC6_dup	134-86	676.05	3.485 ± 0.014	132.9 ± 0.4	194.4 ± 1.2	4.323 ± 0.006	0.64
	MC7	134-86	677.40	8.702 ± 0.035	244.4 ± 0.7	296.2 ± 1.8	5.744 ± 0.005	0.21
	MC7_dup	134-86	677.40	8.030 ± 0.032	227.7 ± 0.7	306.8 ± 1.8	6.365 ± 0.009	0.63
	MC8	134-86	680.78	6.137 ± 0.025	213.5 ± 0.6	217.5 ± 1.3	4.539 ± 0.005	0.47
	MC8_dup	134-86	680.78	5.871 ± 0.023	212.3 ± 0.6	207.1 ± 1.2	4.417 ± 0.005	0.54
MC9	134-86	683.60	4.070 ± 0.016	129.0 ± 0.4	258.3 ± 1.5	5.581 ± 0.006	0.68	
MC10	134-86	691.23	6.570 ± 0.026	184.9 ± 0.6	300.6 ± 1.8	5.993 ± 0.004	0.35	
Serra do Garrote Fm.	G1	134-86	824.37	16.02 ± 0.07	578.7 ± 1.2	222.5 ± 1.5	5.257 ± 0.003	0.19
	G1_dup	134-86	824.37	15.63 ± 0.07	588.7 ± 1.2	212.7 ± 1.4	5.209 ± 0.005	0.19
	G2	134-86	824.42	11.56 ± 0.06	370.1 ± 0.7	274.9 ± 2.1	6.468 ± 0.006	0.20
	G2_dup	134-86	824.42	11.72 ± 0.06	356.8 ± 0.7	300.4 ± 2.3	7.017 ± 0.006	0.17
	G3	134-86	824.76	1.093 ± 0.012	60.6 ± 0.1	116.2 ± 1.5	2.724 ± 0.003	0.07
	G3_dup	134-86	824.76	1.038 ± 0.012	80.2 ± 0.2	76.31 ± 1.00	1.844 ± 0.002	0.10
	G4	134-86	825.83	11.97 ± 0.07	355.4 ± 0.7	305.3 ± 2.3	6.892 ± 0.006	-0.07
	G5	134-86	825.86	5.650 ± 0.028	223.5 ± 0.4	189.8 ± 1.3	4.38 ± 0.005	0.06



Table 3

	Depth (m)	FeT	Fecarb	Feox	Femag	Fe-AVS	Fepy	FeHR	FeHR/FeT	Fe-S/FeHR
Morro do Calcário Fm.	749.03	1.521	0.655	0.196	0.154	nd	0.236	1.241	0.816	0.190
	752.35	2.369	0.856	0.268	0.179	nd	0.601	1.904	0.804	0.316
	756.20	3.116	1.442	0.463	0.305	0.002	0.155	2.365	0.759	0.066
	759.55	2.235	0.324	0.063	0.062	nd	0.072	0.521	0.233	0.138
	764.47	2.132	0.302	0.104	0.061	0.004	0.075	0.542	0.254	0.146
	769.75	2.243	0.725	0.194	0.116	nd	0.094	1.129	0.503	0.083
	774.20	2.221	0.077	0.075	0.030	nd	0.031	0.213	0.096	0.146
	779.10	2.015	0.077	0.038	0.023	nd	0.005	0.143	0.071	0.035
	783.10	0.944	0.527	0.145	0.093	0.002	0.137	0.902	0.956	0.154
	788.15	3.169	0.608	0.129	0.157	nd	1.499	2.393	0.755	0.626
	793.70	0.502	0.359	0.082	0.025	nd	0.001	0.467	0.930	0.002
	799.10	2.301	1.032	0.220	0.307	nd	0.384	1.943	0.844	0.198
	799.25	3.564	0.012	0.031	0.011	nd	2.077	2.131	0.598	0.975
	799.39	2.442	0.011	0.025	0.008	nd	1.344	1.388	0.568	0.968
	799.97	1.717	0.600	0.178	0.265	nd	0.064	1.107	0.645	0.058
	800.12	1.199	0.322	0.079	0.067	nd	0.526	0.994	0.829	0.529
	800.60	4.938	0.007	0.023	0.007	nd	1.069	1.106	0.224	0.967
	801.34	1.542	0.004	0.020	0.007	nd	0.517	0.548	0.355	0.943
	802.67	2.133	0.008	0.027	0.005	nd	0.899	0.939	0.440	0.957
	803.82	3.392	0.118	0.041	0.043	nd	0.996	1.198	0.353	0.831
	804.43	2.521	0.023	0.027	0.001	nd	0.908	0.959	0.380	0.947
	804.63	3.416	1.128	0.245	0.337	0.004	0.193	1.903	0.557	0.104
	806.02	2.174	0.068	0.036	0.026	nd	0.824	0.954	0.439	0.864
	807.75	3.483	0.381	0.101	0.145	nd	0.561	1.188	0.341	0.472
	808.32	2.961	0.160	0.040	0.048	nd	0.653	0.901	0.304	0.725
	809.12	3.319	0.178	0.080	0.064	nd	0.793	1.115	0.336	0.711
	810.15	1.739	0.184	0.069	0.059	nd	0.443	0.755	0.434	0.587
	810.55	4.605	0.233	0.085	0.074	nd	1.674	2.066	0.449	0.810
	811.75	1.802	0.088	0.054	0.044	nd	0.668	0.854	0.474	0.782
	813.05	3.071	0.208	0.072	0.095	nd	0.168	0.543	0.177	0.309
	814.17	2.329	0.148	0.063	0.033	nd	0.814	1.058	0.454	0.769
	814.53	1.858	0.032	0.041	0.013	nd	0.314	0.400	0.215	0.785
	815.08	3.138	1.102	0.291	0.256	0.006	0.693	2.342	0.746	0.298
	816.95	2.082	0.018	0.022	0.002	nd	0.064	0.106	0.051	0.604
	818.00	2.353	0.563	0.128	0.169	nd	0.439	1.299	0.552	0.338
	818.23	0.836	0.278	0.075	0.079	0.007	0.290	0.722	0.864	0.411
	820.20	6.482	0.247	0.076	0.044	nd	1.878	2.245	0.346	0.837
	825.25	0.700	0.381	0.107	0.057	nd	0.085	0.630	0.900	0.135
	830.00	2.768	0.862	0.188	0.196	nd	1.056	2.302	0.832	0.459
	835.40	0.850	0.407	0.088	0.078	nd	0.208	0.781	0.919	0.266